QCD with two light dynamical chirally improved quarks: Baryons

Georg P. Engel, C. B. Lang, Daniel Mohler, and Andreas Schäfer (BGR [Bern-Graz-Regensburg] Collaboration)

Phys. Rev. D **87**, 074504 — Published 22 April 2013

DOI: 10.1103/PhysRevD.87.074504

QCD with Two Light Dynamical Chirally Improved Quarks: Baryons

Georg P. Engel,[1,2,*] C. B. Lang,[1,†] Daniel Mohler,[3,4,‡] and Andreas Schäfer[5,§]
(BGR [Bern-Graz-Regensburg] Collaboration)

[1] *Institut für Physik, FB Theoretische Physik, Universität Graz, A–8010 Graz, Austria*
[2] *Dipartimento di Fisica, Università di Milano-Bicocca and INFN, sezione di Milano-Bicocca, I–20126 Milano, Italy*
[3] *Fermi National Accelerator Laboratory, Batavia, Illinois, USA*
[4] *TRIUMF, 4004 Wesbrook Mall Vancouver, BC V6T 2A3, Canada*
[5] *Institut für Theoretische Physik, Universität Regensburg, D–93040 Regensburg, Germany*

We present a study of baryon ground states and low lying excitations of non-strange and strange baryons. The results are based on seven gauge field ensembles with two dynamical light Chirally Improved (CI) quarks corresponding to pion masses between 255 and 596 MeV and a strange valence quark with mass fixed by the Ω baryon. The lattice spacing varies between 0.1324 and 0.1398 fm. Given in lattice units, the bulk of our results are for size $16^3 \times 32$, for two ensembles with light pion masses (255 and 330 MeV) we also use $24^3 \times 48$ lattices and perform an infinite volume extrapolation. We derive energy levels for the spin 1/2 and 3/2 channels for both parities. In general, our results in the infinite volume limit compare well with experiment. We analyze the flavor symmetry content by identifying the singlet/octet/decuplet contributions of the resulting eigenstates. The ground states compositions agree with quark model expectations. In some cases the excited states, however, disagree and we discuss possible reasons.

PACS numbers: 11.15.Ha, 12.38.Gc

I. INTRODUCTION

Restricting to strong interactions, almost all of the hadrons are resonances. For lattice studies, due to the finiteness of the lattice volumes the smallest momenta come in units $2\pi/L$. Moreover, for unphysically heavy pion masses decay channels are often not open or the resulting phase space is small, leading to energy levels in the vicinity of the resonance energy. This motivates the identification of the low energy levels with masses of corresponding resonances. Eventually, towards physical pion masses and larger lattices, the interpretation becomes invalid and the observed energy levels show a more intricate pattern, related in the elastic channel to two-hadron states [1, 2]. Recent work, where correlators of only single hadron operators were studied [3–5], found no clear signal of possibly coupling two-hadron states (with the possible exception of s wave channels). It was concluded that for a full study one should include such interpolators explicitly. In [6, 7] it was demonstrated in meson correlation studies, that neglect of two-meson interpolators may obscure the obtained energy level picture in some cases. Attempts towards including meson-baryon interpolators are discussed in [8, 9] and a recent study including πN interpolators in the negative parity nucleon sector demonstrated significant effects in the observed energy spectrum [10].

The present work is a continuation of a study of single baryon correlators, with more ensembles and larger statistics as compared to [4]. Like before we see no obvious signal of coupling meson-baryon channels (with a few possible exceptions where the meson-baryon system is in s wave, as will be discussed). We therefore identify the lowest energy levels with baryon ground states and excitations.

We use two mass identical light quarks with the Chirally Improved (CI) fermion action [4, 11, 12]. The strange quark is considered as valence quark, its mass fixed by setting the Ω-mass to its physical value. The pion masses for the seven ensembles of 200–300 gauge configurations each range from 255 MeV to 596 MeV, with lattice size $16^3 \times 32$ and lattice spacing between 0.1324 and 0.1398 fm. For two ensembles with light pion masses also lattices of size $12^3 \times 24$ and $24^3 \times 48$ were used to allow extrapolation to infinite volume.

Other recent studies aiming at light and strange baryon excitations, some of them with 2+1 dynamical quarks, include [3, 13–23]. In [24] excited spectra for non-strange and strange baryon are derived from anisotropic lattices and standard improved Wilson fermions. See also recent reviews [25–27] and references therein.

In Sect. II we discuss the setup for our simulations and remark on the methods used for the data analysis. Results from the $16^3 \times 32$ lattices for light and strange baryons are presented in Sections III and IV respectively. In Sect. V the infinite volume extrapolation and uncertainties with regard to the strange quark mass chosen in our simulations are discussed. We conclude with a summary in Sect. VI.

*Electronic address: georg.engel@mib.infn.it
†Electronic address: christian.lang@uni-graz.at
‡Electronic address: dmohler@fnal.gov
§Electronic address: andreas.schaefer@physik.uni-regensburg.de

II. SETUP OF THE SIMULATION AND ANALYSIS

The CI fermion action [11, 12] results from a parametrization of a general fermion action connecting each site along gauge link paths to other sites up to distance three (in lattice units). This truncated ansatz is used to algebraically solve the Ginsparg-Wilson equation. The action consists of several hundred terms and obeys the Ginsparg-Wilson relation approximately. It was used in quenched [28, 29] and dynamical simulations [30]. It was found that the small eigenvalues fluctuate predominantly towards the inside of the Ginsparg-Wilson unit circle [31]. Exceptionally small eigenvalues are suppressed, which allows to simulate smaller pion masses on coarse lattices. For further improvement of the fermion action one level of stout smearing of the gauge fields [32] was included in its definition. The parameters are adjusted such that the value of the plaquette is maximized ($\rho = 0.165$ following [32]). For the pure gauge field part of the action we use the tadpole-improved Lüscher-Weisz gauge action [33]. For a given gauge coupling we use the same assumed plaquette value for the different values of the bare quark mass parameter.

The lattice spacing a is defined as discussed in [34], using the static potential with a Sommer parameter $r_0 = 0.48$ fm and setting the scale at the physical pion mass for each value of β_{LW}. This value of the Sommer parameter may be slightly too small for $n_f = 2$, as has been argued recently [35, 36], where a value near 0.5 fm is preferred.

All parameters as well as details of the implementation in the Hybrid Monte Carlo simulation [30, 37] and various quality check are given in [4, 34]. For reference we summarize the parameters of the used gauge field ensembles in Table I.

In each baryon channel with given quantum numbers the eigenenergy levels are determined with the so-called variational method [38, 39]. One uses interpolators with the correct symmetry properties and computes the cross-correlation matrix $C_{ik}(t) = \langle O_i(t) O_k(0)^\dagger \rangle$. One then solves the generalized eigenvalue problem

$$C(t)\vec{u}_n(t) = \lambda_n(t) C(t_0)\vec{u}_n(t) \qquad (1)$$

in order to approximately recover the energy eigenstates $|n\rangle$. The exponential decay of the eigenvalues

$$\lambda_n(t) = \mathrm{e}^{-E_n\,(t-t_0)}(1 + \mathcal{O}(\mathrm{e}^{-\Delta E_n (t-t_0)})) \qquad (2)$$

allows us to obtain the energy values, where ΔE_n is the distance to other spectral values. In [40] it was shown that for $t_0 \le t \le 2t_0$ the value of ΔE_n is the distance to the first neglected eigenenergy. In an actual computation the statistical fluctuations limit the values of t_0 and one estimates the fit range by identifying plateaus of the effective energy. The eigenvectors serve as fingerprints of the states, indicating their content in terms of the lattice interpolators.

The quality of the results depends on the statistics and the set of lattice operators. The dependence on t_0 is studied. Larger values of t_0 increase the noise and reduce the possible fit range, although the results are consistent. In the final analysis we use $t_0 = 1$ (with the origin at 0). The statistical error is determined with single-elimination jack-knife. For the fits to the eigenvalues (2) we use single exponential behavior but check the stability with double exponential fits; we take the correlation matrix for the correlated fits from the complete sample [34]. As an example we show eigenvalues for the four lowest states in the $\Sigma\ 1/2^+$ channel for three ensembles in Fig. 1. In general, we find very good agreement between the eigenstates of all considered ensembles. This suggests the interpretation of a signal with physical origin and in some cases serves to justify a fit relying on only few points.

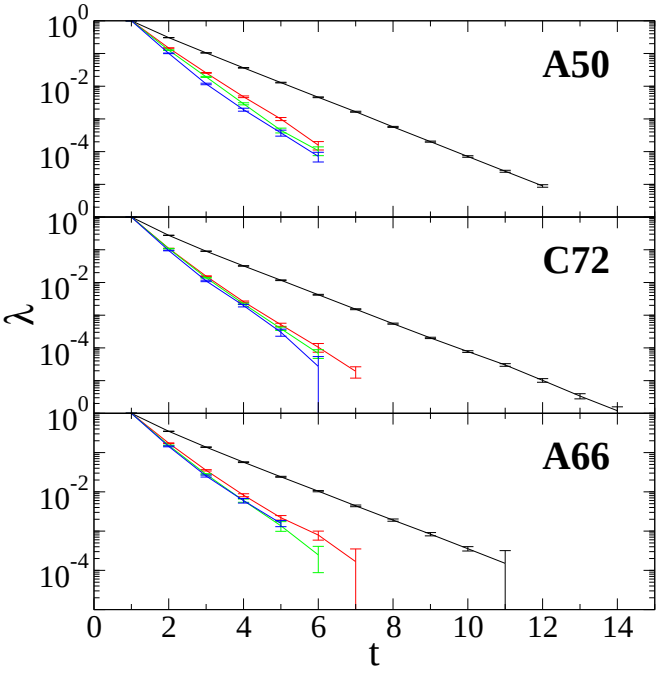

FIG. 1: Eigenvalues for the four lowest states in the $\Sigma\ 1/2^+$ channel for ensembles A50, C72 and A66 (top to bottom) which covers the whole range of pion masses considered.

The set of interpolators used should be capable to approximate the eigenstates. On the other hand, too large a set may add statistical noise. In practice one tries to reduce the number of interpolators to a sufficient subset. We analyze the dependence of the energy levels on the choice of interpolators and fit ranges for the eigenvalues. For the final result, we make a reasonable choice of interpolators and fit range and discuss the associated systematic error. For the extrapolation towards the physical pion mass we fit to the leading order chiral behavior, i.e., linear in m_π^2.

The Dirac and flavor structure is motivated by the quark model [41, 42], see also [43]. Within the relativistic quark model there have been many determinations of the hadron spectrum, based on confining potentials and different assumptions on the hyperfine interaction (see, e.g., [44–46]). The singlet, octet and decuplet attribu-

set	β_{LW}	m_0	m_s	configs.	m_π [MeV]	$L^3 \times T\,[a^4]$	$m_\pi L$	a [fm]
A50	4.70	-0.050	-0.020	200	596(5)	$16^3 \times 32$	6.40	0.1324(11)
A66	4.70	-0.066	-0.012	200	255(7)	$16^3 \times 32$	2.72	0.1324(11)
B60	4.65	-0.060	-0.015	300	516(6)	$16^3 \times 32$	5.72	0.1366(15)
B70	4.65	-0.070	-0.011	200	305(6)	$16^3 \times 32$	3.38	0.1366(15)
C64	4.58	-0.064	-0.020	200	588(6)	$16^3 \times 32$	6.67	0.1398(14)
C72	4.58	-0.072	-0.019	200	451(5)	$16^3 \times 32$	5.11	0.1398(14)
C77	4.58	-0.077	-0.022	300	330(5)	$16^3 \times 32$	3.74	0.1398(14)
LA66	4.70	-0.066	-0.012	97		$24^3 \times 48$	4.08	0.1324(11)
SC77	4.58	-0.077	-0.022	600		$12^3 \times 24$	2.81	0.1398(14)
LC77	4.58	-0.077	-0.022	153		$24^3 \times 48$	5.61	0.1398(14)

TABLE I: Parameters of the simulation: Ensemble names are given in the first row. We show the gauge couplings β_{LW}, the light quark mass parameter m_0, the strange quark mass parameter m_s, the number of configurations analyzed ("configs."), the pion mass and the volume $L^3 \times T$ in lattice units. The dimensionless product of the pion mass with the spatial extent of the lattice, $m_\pi L$, enters finite volume corrections. We also give the lattice spacing a as discussed in [34]. The three ensembles LA66, SC77 and LC77 are separated from the others by a horizontal line, since they are used only for a discussion of finite volume effects. For these ensembles we use the pion masses of A66 and C77, respectively.

tion [43] of the states has been evaluated based on such model calculations, e.g., in [47] (see also the summary in [48]). We use sets of up to 24 interpolating fields in each quantum channel, combining quark sources of different smearing widths, different Dirac structure and octet and decuplet flavor structure. In Appendix A we summarize the structure and numbering of the baryon interpolators used in this study.

III. RESULTS FOR LIGHT BARYONS

A. Nucleon

$\mathbf{N}:\ \mathbf{I}(\mathbf{J^P}) = \frac{\mathbf{1}}{\mathbf{2}}(\frac{\mathbf{1}}{\mathbf{2}}^+)$: The nucleon (spin 1/2 and positive parity) ground state is the lightest baryon. We use a $n_{\rm op} \times n_{\rm op}$ correlation matrix with $n_{\rm op} = 6$ interpolators covering three Dirac structures and different levels of quark smearing, (1,2,9,10,19,20) (see Appendix A), and extract the four lowest eigenstates. For the ground state the leading order chiral extrapolation yields a mass value roughly 7% larger than the experimental N (see Fig. 2). Part of the deviation is caused by finite volume effects, which will be discussed in Section V. The remaining small deviation might be caused by systematic errors from scale setting (using $r_0 = 0.48$ fm), or a curvature due to higher order terms in the chiral extrapolation (for a discussion on the latter, see, e.g., [36]). Within the basis used in the variational method, the ground state is dominated by the first Dirac structure, with a contribution of the third one (cf., Table III). We stress that all Dirac structures used here generate independent field operators which are not related by Fierz transformations.

The first excitation in the nucleon channel should be the "Roper resonance $N(1440)$", notorious because it lies below the ground state in the corresponding negative parity channel. This "reverse level ordering" differs from the expectations of most simple quark models (see, e.g., [42, 49]). However, in our simulation, the first excitation is $\mathcal{O}(500$ MeV) higher than the experimental value. The levels are ordered conventionally with alternating parity. This is also the case in lattice simulation with quenched and dynamical results of other groups (e.g.,[3, 50, 51]). Towards physical pion masses, the first excitation was reported to bend down significantly [18], however, still all lattice results are closer to the $N(1710)$ than to the Roper resonance $N(1440)$, with large error bars.

At present it is unclear to us, what the reason for this behavior may be, although there are several suspects. Finite volume effects could shift the energy level up. For the ground state this shift is comparatively small (as discussed in Section V). This could be significantly larger for the excited state, which is generally expected to have larger physical size. (E.g., in quark models it is considered as a radial excitation.) Unfortunately, the signal of this state is too weak in our study to allow for a reliable analysis of finite volume effects.

Another interpretation may be that the used interpolators may not couple strongly enough to the Roper resonance and thus represent the physical content poorly and we might even miss the physical Roper state altogether. We observe a similar problem in the corresponding Lambda sector [5]. There the first observed excitation is dominated by singlet interpolators (first Dirac structure) matching the $\Lambda(1810)$ (singlet in the quark model). The Roper-like $\Lambda(1600)$ (octet in the quark model) seems to be missing.

Furthermore, the energy levels of the p-wave scattering state πN also could influence the situation dramatically. Inclusion of such baryon-meson interpolator may be necessary for a better representation of the physical state.

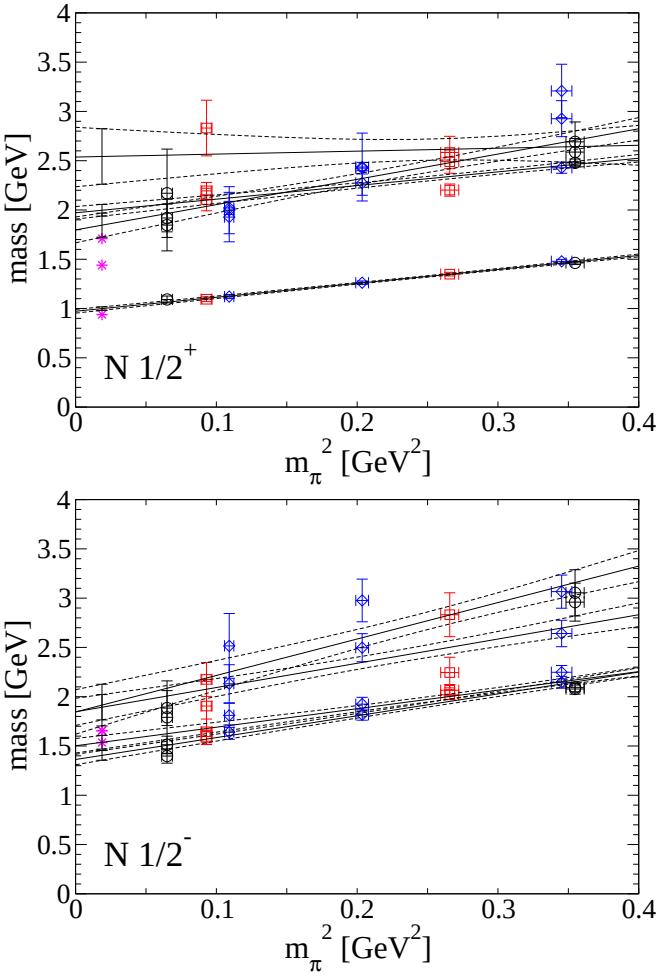

FIG. 2: Energy levels for nucleon spin 1/2, positive (upper) and negative parity (lower). Black, red and blue (color online) denote a value of β equal to 4.70, 4.65 and 4.58, respectively. The solid lines give the mean values of the fits in m_π^2, the dashed ones indicate the region of one σ.

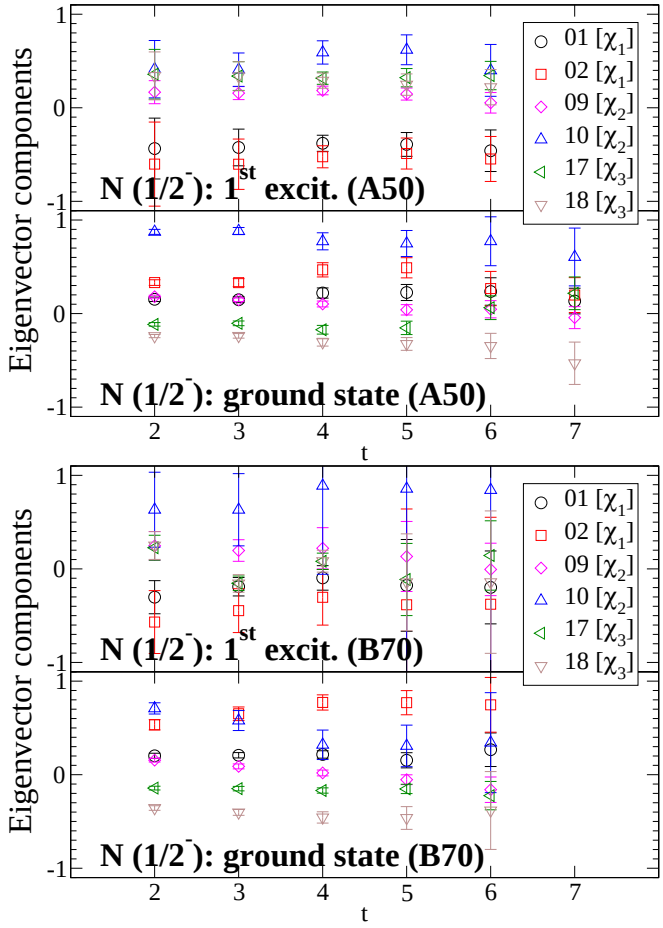

FIG. 3: Eigenvectors for nucleon spin 1/2 negative parity ground state and first excitation, ensemble A50 (upper) and B70 (lower). Note the different composition of the states at the different pion masses.

The resulting energy spectrum is related to the scattering phase shift in this channel [8, 9]. In small boxes and for broad resonances, the resulting energy levels are shifted significantly with regard to noninteracting levels and the resonance mass has to be extracted from the phase shift data. As the experimental Roper state is broad this shift might be significant.

After chiral extrapolation, we obtain two close excitations within roughly 1800-2000 MeV. One of those has a χ^2/d.o.f. of the fit of larger than three (see Table V), which may suggests a non-linear dependence on m_π^2. However, an extrapolation using only data with pion masses below 350 MeV misses the experimental Roper resonance as well.

In several of our ensembles the excited energy levels overlap with each other within error bars. At light pion masses, the first excitation is dominated by a combination of interpolators of the second Dirac structure; the second excitation is dominated by the first Dirac structure, with some contribution from the third one. Towards heavier quark masses, this level ordering interchanges.

Finally, we note that the results in the nucleon positive parity channel do not deviate significantly from the corresponding quenched simulations [29].

N : $\mathbf{I(J^P) = \frac{1}{2}(\frac{1}{2}^-)}$: In general, we find somewhat low energy levels in the negative parity baryon channels, compared to experiment. This is also true for the nucleon spin 1/2 negative parity channel. We use again the set of interpolators (1,2,9,10,19,20), and find that the chiral extrapolation of the ground state comes out too low and that of the first excitation ends up near the experimental ground state mass value (see Fig. 2).

The two lowest states are usually identified with the N(1535) and N(1650). However, in that channel the $N\pi$ state is in s wave. A naive estimate of its energy (neglecting the interaction energy) at values of the pion mass above 300 MeV puts it close to the observed lowest energy level. Towards small pion masses the $N\pi$ energy level should fall more steeply than the nucleon mass to-

wards the physical point. This suggests a (avoided) level crossing of the (negative parity) nucleon and the $N\pi$ state with related energy level shifts, when moving from larger to smaller pion energies.

Indeed, our results are compatible with such a picture. In [4] we analyzed only a subset of the configurations available in this work. There, we argued that the eigenvectors show no indication for a level crossing in the range of pion masses between roughly 300 and 600 MeV. In the present work, we can monitor the eigenvectors down to pion masses of 250 MeV. Furthermore, we use a larger basis (at the cost of introducing additional noise.) We use the same quark smearing structures for different Dirac structures, such that the eigenvectors give information about the content of the state without the need of additional normalization of the interpolators. We find indeed a significant change in the eigenvectors towards lighter pion masses. The eigenvectors are shown for ensembles A50 and B70 in Fig. 3. In particular, the ground state is dominated by interpolator 2 (χ_1) around $m_\pi = 300$ MeV, and by interpolator 10 (χ_2) above $m_\pi = 500$ MeV. For the first excitation, interpolator 10 contributes stronger at lighter pion masses compared to heavier ones. This trend is observed also in the other ensembles and at partially quenched data. However, the picture does not clearly support an (avoided) level crossing scenario, a unique conclusion is missing.

The observed behavior towards smaller quark masses was also discussed in [21] for the 2+1 flavor situation. A recent simulation including (for the first time) also πN interpolators [10] demonstrated significant changes on the spectrum. In that light we may interpret the states obtained in the present study (with only 3-quark interpolators), as effective superpositions of resonance and meson baryon states.

We postpone further discussion of the content of the states to Section V, where finite volume effects will be discussed.

N : $\mathbf{I(J^P) = \frac{1}{2}(\frac{3}{2}^+)}$: In the nucleon spin 3/2 positive parity channel, three states are known experimentally: The $N(1720)$, $N(1900)$ and $N(2040)$, where the latter needs confirmation [48]. We use interpolators (1,4,5), respectively (1,2,3,4) in A66 and B70. The signal is rather noisy and the effective mass plateaus appear to fall towards large time separations. Sizable deviations from the chiral fit are observed in ensembles B70 and C77. Nevertheless, the chiral extrapolation of the ground state agrees well with the experimental $N(1720)$ (see Fig. 4). The first excitation overshoots the $N(1900)$ by about 2σ, which thus cannot be confirmed from this study.

N : $\mathbf{I(J^P) = \frac{1}{2}(\frac{3}{2}^-)}$: In this channel, experimentally, $N(1520)$, $N(1700)$ and $N(1875)$ are established. Using interpolators (1,2,3,4), three states can be extracted in our simulation (see Fig. 4). The ground state extrapolates to a value between the $N(1520)$ and the $N(1700)$, the first and second excitation come out higher than

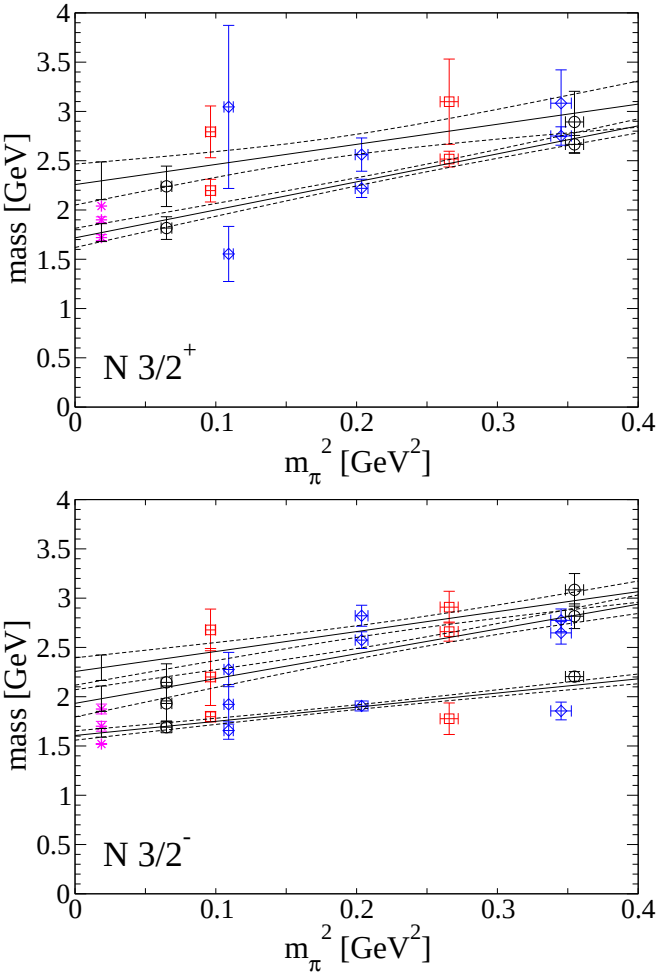

FIG. 4: Energy levels for nucleon spin 3/2, positive (upper) and negative parity (lower).

$N(1700)$ or $N(1875)$.

B. Delta

Δ : $\mathbf{I(J^P) = \frac{3}{2}(\frac{1}{2}^+)}$: Experimentally, the ground state $\Delta(1750)$ still needs confirmation, while $\Delta(1910)$ is well established. In our simulation, using interpolators (1,4,5), we find two states, where the second eigenvalue decreases slower with the pion mass than the first one. The resulting crossing of the eigenvalues complicates the analysis and one has to follow the eigenvector composition in order to properly assign the state. However, the plateaus can be fitted and energy levels extracted, albeit with sizable error bars. The chiral extrapolation of the ground state is compatible with both $\Delta(1750)$ and $\Delta(1910)$ within the error bars, the first excitation comes out higher (see Fig. 5).

Δ : $\mathbf{I(J^P) = \frac{3}{2}(\frac{1}{2}^-)}$: In the negative parity channel,

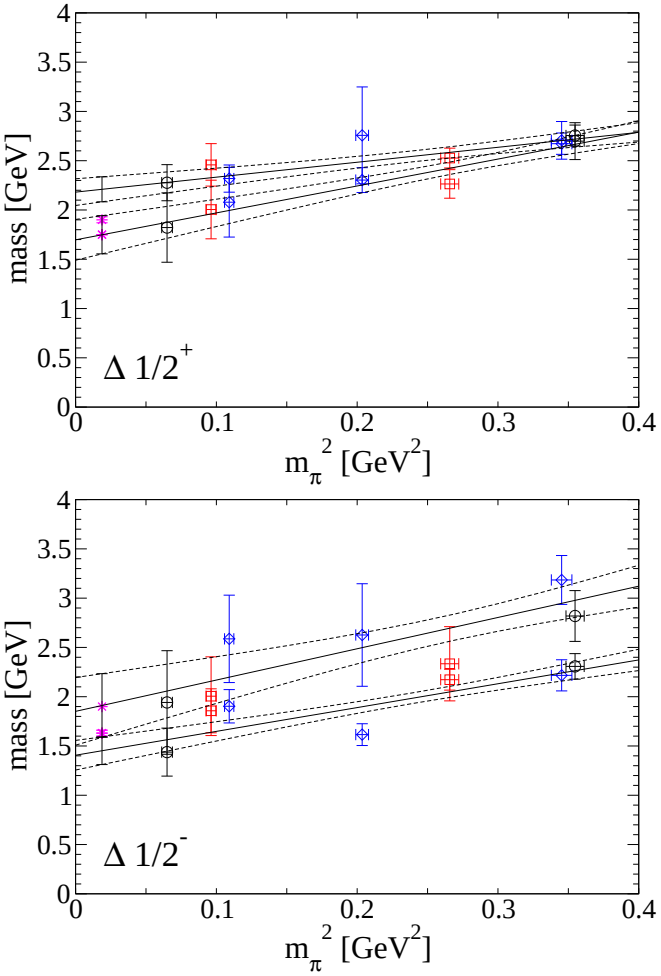

FIG. 5: Energy levels for Δ spin 1/2, positive (upper) and negative parity (lower).

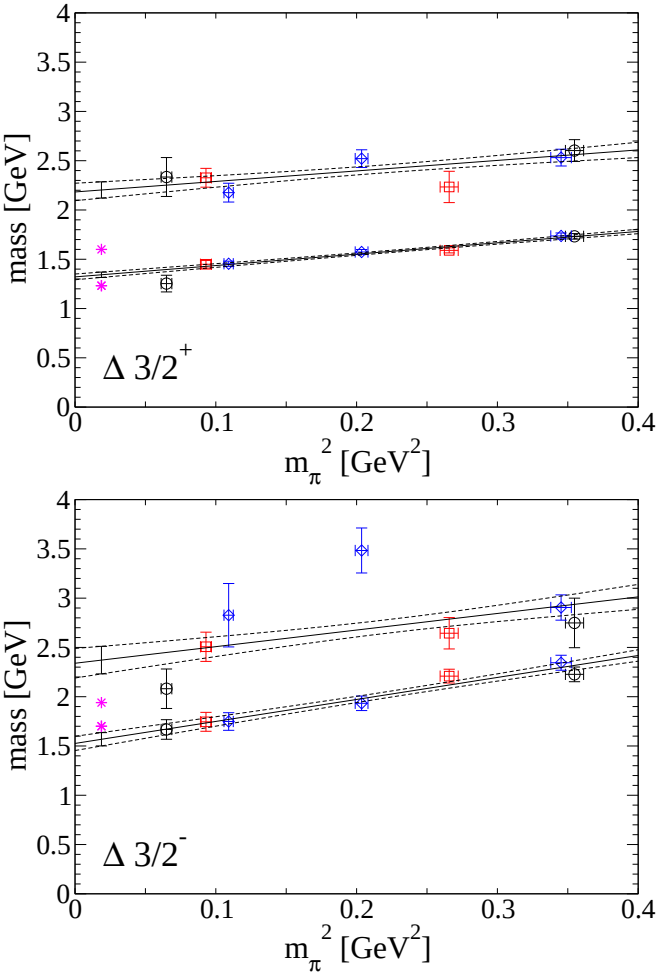

FIG. 6: Energy levels for Δ spin 3/2, positive (upper) and negative parity (lower).

$\Delta(1620)$ is established, while $\Delta(1900)$ needs confirmation. Using interpolators (1,2,3,4) we extract two states in this channel. The chiral extrapolation of the ground state hits the experimental $\Delta(1620)$ within 1.2σ (see Fig. 5). The excitation extrapolates to the $\Delta(1900)$, however, with a large associated error.

Δ : $\mathbf{I(J^P) = \frac{3}{2}(\frac{3}{2}^+)$: The $\Delta(1232)$ is the lowest resonance of all spin 3/2 baryons. We find a good signal of two states, the chiral extrapolations of both come out too high compared to the experimental $\Delta(1232)$ and the $\Delta(1600)$ (see Fig. 6). Finite volume effects are a possible origin of the discrepancy, as will be discussed in Section V. A possible p-wave energy of a coupling $N\pi$ state would lie between the two observed levels and is not seen. Note that the partially quenched data of this channel are used to set the strange quark mass parameter [34].

Δ : $\mathbf{I(J^P) = \frac{3}{2}(\frac{3}{2}^-)$: We find a good signal in the $J^P = 3/2^-$ Δ channel in all seven ensembles (see Fig. 6). However, like in other negative parity baryon channels, the chiral extrapolation of the ground state comes out rather low compared to experiment. The results for the first excitation are inconclusive, the χ^2/d.o.f. of the chiral extrapolation fit is larger than three.

IV. RESULTS FOR STRANGE BARYONS

A. Lambda

Lambda baryons come as flavor singlets or octets, or as mixtures of them. Lattice simulations in this channel are of particular interest, as for years no state was observed in the vicinity of the prominent low-lying $\Lambda(1405)$ (see, e.g., [52, 53]). Only recent results show a level ordering compatible with experiment [20]. Our results for the Lambda baryons have been discussed elsewhere [5]. Here a few observations are summarized for completeness.

We include interpolators of flavor singlet and octet type and three Dirac structures in all four $J^P = \frac{1}{2}^\pm$ and $\frac{3}{2}^\pm$ channels. In both 1/2 channels and in the $\frac{3}{2}^+$

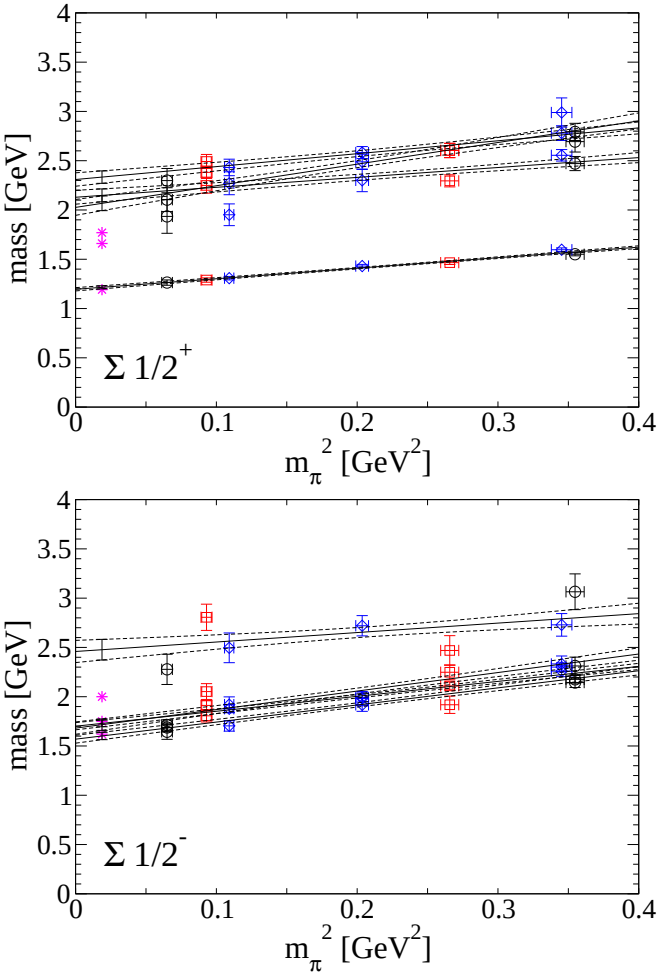

FIG. 7: Energy levels for Σ spin 1/2, positive (upper) and negative parity (lower).

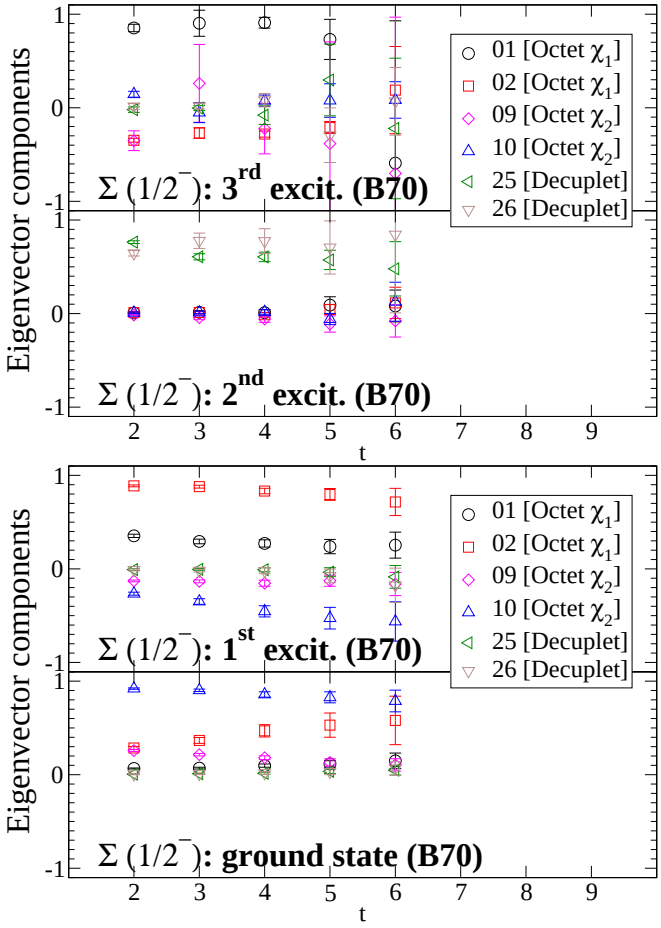

FIG. 8: Eigenvectors for Σ spin 1/2 negative parity ground state and first excitation (upper) and second and third excitation (lower) for ensemble B70. Note the dominance of decuplet interpolators for the second excitation, which is a low lying state (see Fig. 7). Details are discussed in the text.

channel we find ground states extrapolating to the experimental values, whereas the $\frac{3}{2}^-$ ground state comes out too high. We confirm the $\Lambda(1405)$ and also find two low-lying excitations in the $\frac{1}{2}^-$ channel. Our results suggest that the $\Lambda(1405)$ is dominated by flavor singlet 3-quark content, but at $m_\pi \approx 255$ MeV octet interpolators contribute roughly 15-20%, which may increase towards physical pion masses. The Roper-like (octet) state $\Lambda(1600)$ may couple too weak to our 3-quark interpolator basis. We analyze the volume dependence and find that only the spin $\frac{1}{2}^+$ ground state shows a clear exponential dependence as expected for bound states. For all other discussed states, the volume dependence is either fairly flat or obscured by the statistical error.

B. Sigma

$\mathbf{\Sigma:\ I(J^P) = 1(\frac{1}{2}^+)}$: The $\Sigma(1189)$ ground state marks one of the lowest energy levels of the spin 1/2 baryons. At the $SU(3)$ flavor symmetric point, the octet and decuplet irreducible representations are orthogonal. Towards physical quark masses, $SU(3)_f$ is broken and hence octet and decuplet are allowed to mix. We use the set (1,2,9,10,25,26), which includes octet interpolators with Dirac structures χ_1 and χ_2 and decuplet interpolators in the basis. We use the four lowest levels for our analysis. The eigenvalues for three ensembles are shown in Fig. 1. The ground state signal is fairly good and the chiral extrapolation results in a value close to the experimental $\Sigma(1189)$ (see Fig. 7). The first excitation comes out too high compared to the experimental $\Sigma(1660)$. Note the poor χ^2/d.o.f. of the corresponding chiral extrapolation, with a value larger than four (see Table V). The energy levels of the second and third excitations appear close to the first excitation in our simulations.

Monitoring the eigenvectors, we analyze the octet/decuplet content of the states. Within the finite basis employed, the ground state and the first excitation are strongly dominated by octet χ_1. Of

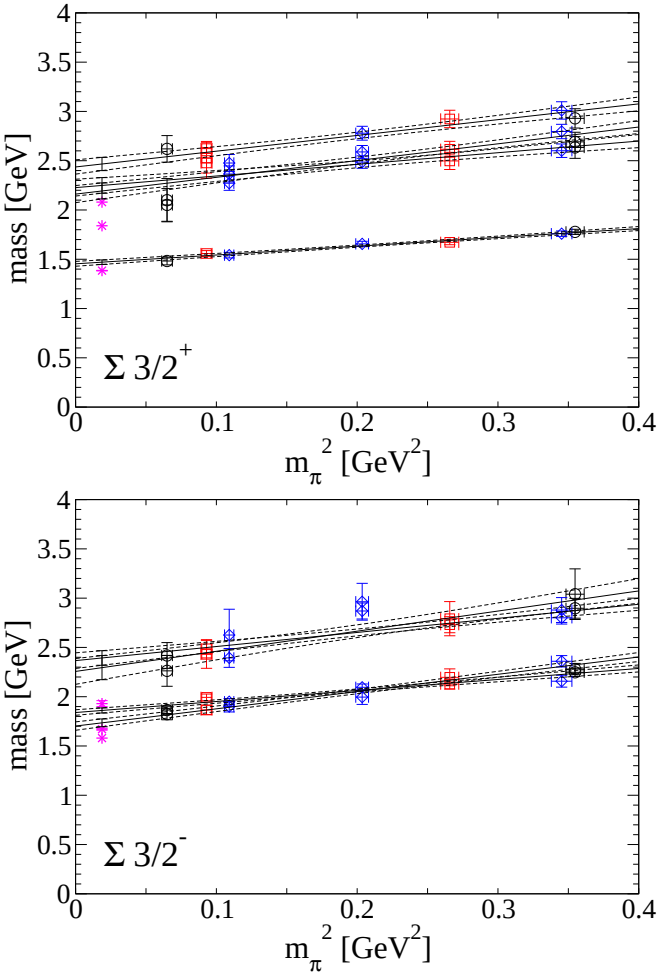

FIG. 9: Energy levels for Σ spin 3/2, positive (upper) and negative parity (lower).

the second and third excitation, one is dominated by decuplet and the other by octet χ_2 interpolators. The mixing of octet and decuplet interpolators is found to be negligible in the range of pion masses considered. As we will see, this holds for most Σ and Ξ channels discussed here.

Σ : $\mathbf{I(J^P) = 1(\frac{1}{2}^-)}$: In the Σ spin 1/2 negative parity channel, the Particle Data Group [48] lists two low nearby states, Σ(1620) and Σ(1750), and one higher lying resonance, the Σ(2000). Of those, only Σ(1750) is established.

Again the set of interpolators (1,2,9,10,25,26) is used to extract four lowest states from our simulations. We find three low nearby states, all of which extrapolate close to the experimental Σ(1620) and Σ(1750) (see Fig. 7). Hence, our results confirm the Σ(1620) and Σ(1750) and even might suggest the existence of a third low lying resonance. However, as discussed for the N($\frac{1}{2}^-$) (and like in the case of the Λ($\frac{1}{2}^-$)) there are several s wave baryon-meson channels ($N\overline{K}$, $\Lambda\pi$, $\Sigma\pi$), which, for our values of the pion mass, have energies close to the ground state. We cannot exclude such contributions, although we did not include them in the interpolators.

The eigenvectors of all four states are shown for ensemble B70 in Fig. 8. Within the employed basis, the ground state is dominated by octet χ_2, the first excitation by octet χ_1, the second excitation by decuplet and the third excitation again by octet χ_1 interpolators. We want to emphasize the existence of a low lying state in this channel which is dominated by decuplet interpolators. This result also agrees with a recent quark model calculation [47]. Again, the mixing of octet and decuplet interpolators appears to be negligible in the range of pion masses considered.

Σ : $\mathbf{I(J^P) = 1(\frac{3}{2}^+)}$: The Particle Data Group lists Σ(1385), Σ(1840) and Σ(2080), where only the lightest is established. We use interpolators (2,3,10,11,12) and extract four energy levels (see Fig. 9). The chiral extrapolations come out high compared to the experimental values. From the eigenvectors we find that the lowest two states are strongly dominated by decuplet, the second excitation by octet and the third excitation again by decuplet interpolators.

Σ : $\mathbf{I(J^P) = 1(\frac{3}{2}^-)}$: In this channel, three states are known experimentally: Σ(1580), Σ(1670) and Σ(1940), where the lightest one needs confirmation. Using interpolators (2,3,10,11,12) we can extract four states. We find two low lying states and two higher excitations (see Fig. 9). In general, the corresponding energy levels are high compared to experiment, thus not confirming the Σ(1580). However, the mixing of octet and decuplet might increase towards light pion masses, complicating the chiral behavior. Analyzing the eigenvectors, we find that of the two low lying states, one is dominated by octet and the other one by decuplet interpolators. Of the third and fourth state, one is dominated by octet and the other by decuplet interpolators. Compared to the other Σ channels, there appears a measurable mixing of octet and decuplet interpolators. We remark the importance of decuplet interpolators for low-lying states in this channel.

C. Xi

Ξ : $\mathbf{I(J^P) = \frac{1}{2}(\frac{1}{2}^+)}$: Experimentally, only one resonance Ξ(1322) is known in the Ξ spin 1/2 positive parity channel. We use interpolators (1,2,9,10,25,26) and extract the four lowest states. The ground state shows a fairly clean signal and its chiral extrapolation agrees nicely with the Ξ(1322) (see Fig. 10). The three excitations come out much higher and the results at the lightest pion mass may suggest a significant chiral curvature towards physical pion masses. This is also expressed in the poor χ^2/d.o.f., which is above five for the first excita-

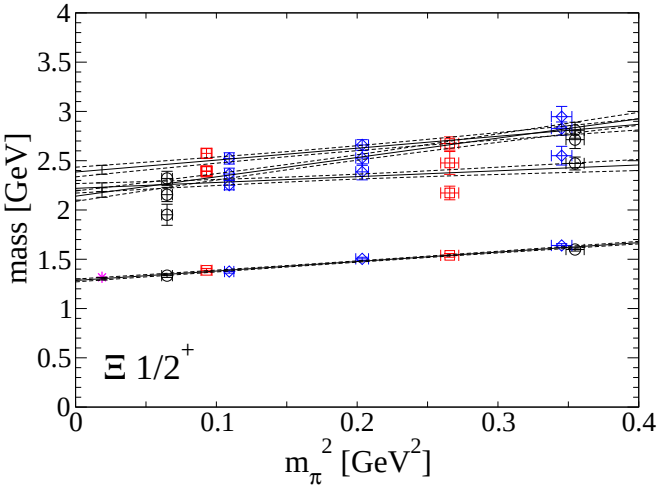

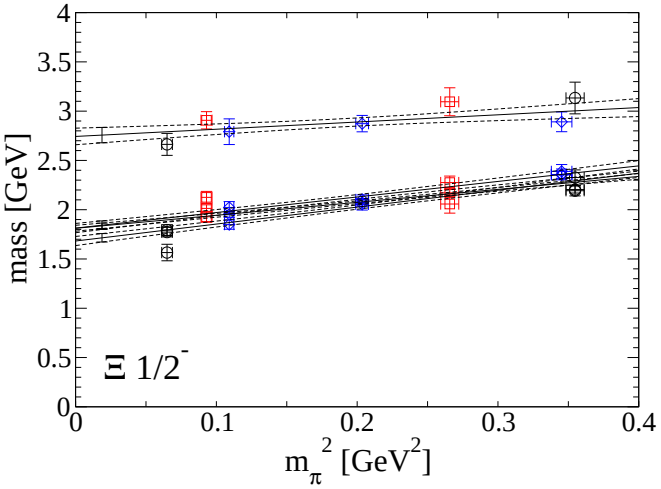

FIG. 10: Energy levels for Ξ spin 1/2, positive (upper) and negative parity (lower).

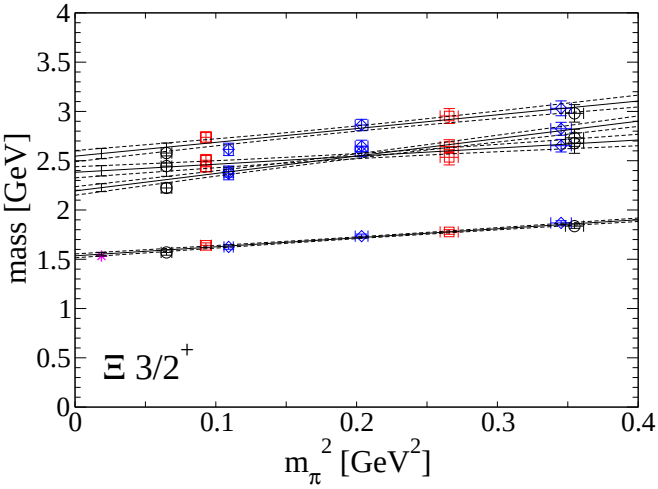

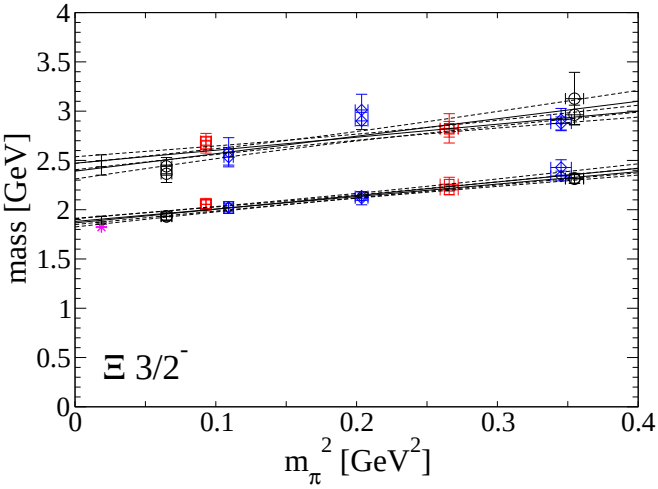

FIG. 11: Energy levels for Ξ spin 3/2, positive (upper) and negative parity (lower).

tion (see Table V). Analyzing the eigenvectors, we find that – within the finite basis used – the ground state and the first excitation are strongly dominated by octet χ_1. Of the third and the fourth excitation, one is dominated by decuplet and the other one by octet χ_2 interpolators. The mixing of octet and decuplet interpolators is found negligible in the range of simulated pion masses.

Ξ : $\mathbf{I(J^P) = \frac{1}{2}(\frac{1}{2}^-)}$: No state is known in the Ξ spin $1/2^-$ channel experimentally, and no low-lying state identified in quark model calculations like, e.g., [47]. Nevertheless, using interpolators (1,2,9,10,25,26), we identify four states in our simulations (see Fig. 10). Of those, three are low lying and extrapolate to 1.7-1.9 GeV. Note the poor χ^2/d.o.f. larger than three of the corresponding three chiral extrapolations. The fourth state appears rather high at 2.7-2.9 GeV, but its extrapolation shows a nice χ^2/d.o.f. of order one. From the eigenvectors we find that the ground state is dominated by octet χ_2, the first excitation by octet χ_1, the second excitation by decuplet and the third excitation again by octet χ_1 interpolators. We emphasize the existence of a low lying state in this channel which is dominated by decuplet interpolators, analogous to the Σ spin 1/2 negative parity channel.

Ξ : $\mathbf{I(J^P) = \frac{1}{2}(\frac{3}{2}^+)}$: In this channel, one state, Ξ(1530), is experimentally known and well established. We use interpolators (2,3,10,11,12) to extract four states from our simulation. All four states show a stable signal and the ground state energy level nicely extrapolates to the experimental Ξ(1530) (see Fig. 11). The second and third energy levels appear rather close to each other and are compatible with a level crossing picture within pion masses of 300-500 MeV. Within the finite basis used, the ground state is dominated by decuplet interpolators, which agrees with quark model calculations. At light pion masses, the first excitation is dominated by octet and the second by decuplet interpolators. The third excitation is again dominated by decuplet interpolators.

Ξ : $\mathbf{I(J^P) = \frac{1}{2}(\frac{3}{2}^-)}$: The Particle Data Group [48] lists one (established) state, Ξ(1820), which is ex-

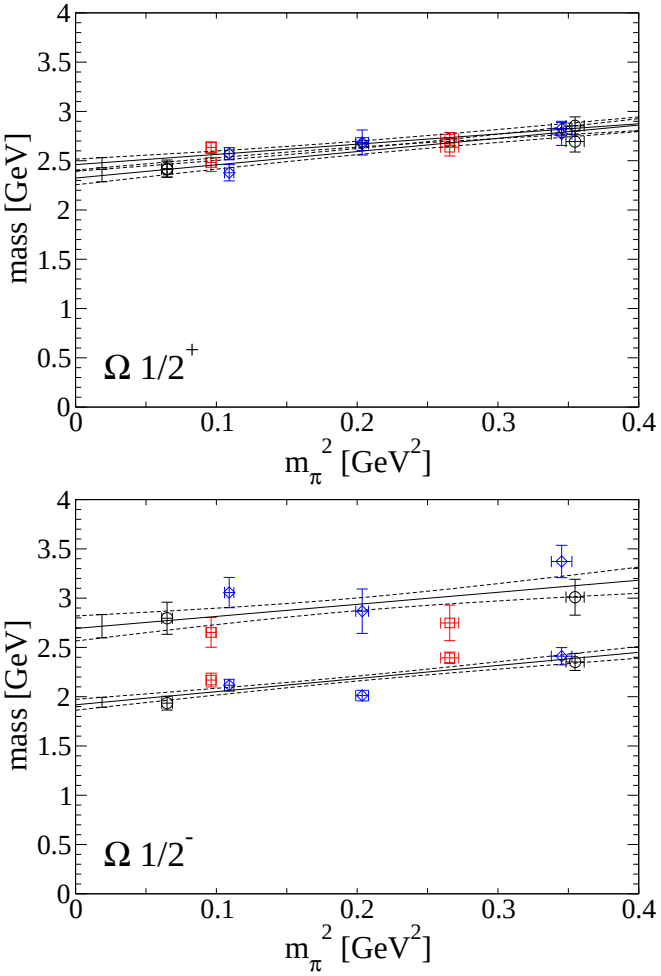

FIG. 12: Energy levels for Ω spin 1/2, positive (upper) and negative parity (lower).

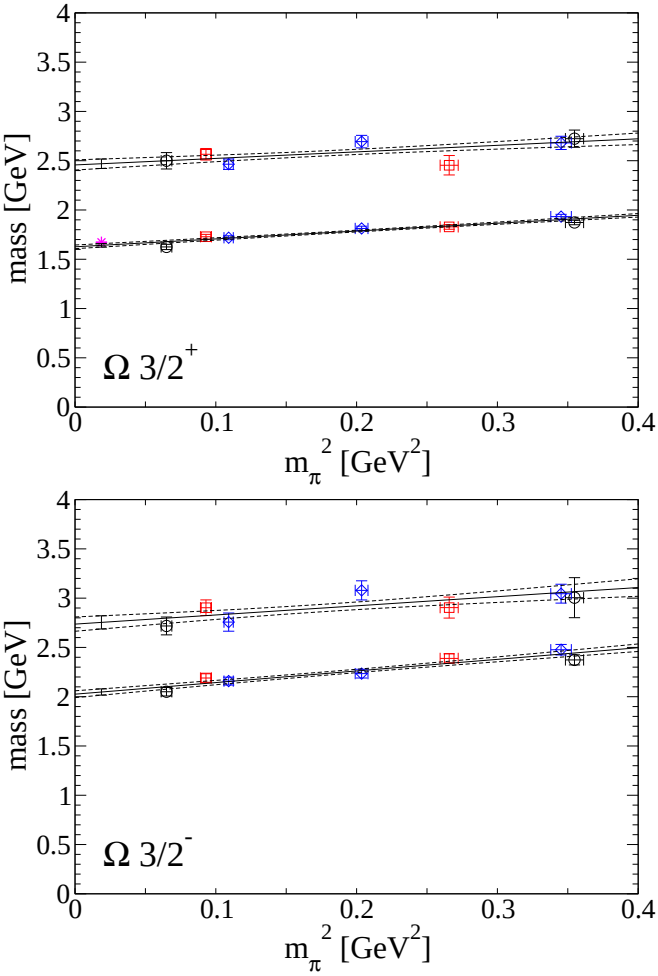

FIG. 13: Energy levels for Ω spin 3/2, positive (upper) and negative parity (lower).

pected to be dominated by octet interpolators according to quark model calculations [48]. Using interpolators (2,3,10,11,12), we extract four energy levels in this channel. We find two low lying states, the energy levels of which extrapolate close to the experimental Ξ(1820) (see Fig. 11). Analyzing the eigenvectors, we find that of the two low lying states, one is dominated by octet and the other one by decuplet interpolators. The third state is dominated by octet and the fourth state by decuplet interpolators. Compared to the other Ξ channels, there appears a small but measurable mixing of octet and decuplet interpolators.

D. Omega

Ω : $\mathbf{I(J^P) = 0(\frac{1}{2}^+)}$: Experimentally, the Ω baryons have been investigated little. No state is known in the $J^P = 1/2^+$ channel. Using the same interpolators as in the corresponding Δ channel, we find two states, whose energy levels are close for all simulated pion masses (see Fig. 12). Both predicted resonances lie between 2.3 and 2.6 GeV.

Ω : $\mathbf{I(J^P) = 0(\frac{1}{2}^-)}$: Again, there is no experimental experience in the $J^P = \frac{1}{2}^-$ channel of the Ω baryons. We extract two states, where the excitation comes with some noise. The chiral extrapolation of the ground state predicts a resonance around 2 GeV (see Fig. 12). Note the corresponding poor χ^2/d.o.f. larger than four (see Table VI); its main contribution comes from the light energy level of one ensemble (C72). Since this behavior is not systematically observed in other channels, we assume the deviation to be due to statistical fluctuations.

Ω : $\mathbf{I(J^P) = 0(\frac{3}{2}^+)}$: The Ω(1672) in the $J^P = 3/2^+$ channel is known experimentally to very high accuracy. This is one of the reasons why this state is often used to define the strange quark mass parameters. This approach is pursued also in our setup. The determination of the parameters has been performed along a different scheme

of scale setting. The Sommer parameter was identified with the experimental value for each ensemble, without extrapolation to physical pion masses. In that scheme the lowest energy level in the Ω $J^P = 3/2^+$ channel was identified with the experimental $\Omega(1672)$ for each ensemble. This identification used preliminary data on the $16^3 \times 32$ lattices only. Here we present results relying on another scheme of scale setting [34]. Thus, the results shown here for the ground state serve as an additional cross check for the final setup of the simulation.

The ground state energy level extrapolates close to the experimental $\Omega(1672)$, undershooting it slightly (see Figure 13). The corresponding χ^2/d.o.f. is around two (see Table V), half of it contributed by ensemble A66. Using our final dataset and revisiting the tuning, we find that the strange quark mass of ensemble A66 is slightly too light while the mass from ensemble C64 is slightly too heavy. This creates a slope in the chiral extrapolation which causes the $\Omega(1672)$ (and to a lesser extent all baryons involving one or more strange quarks) to be lighter than a proper tuning would imply. A thorough discussion is difficult since also other systematics enter. We will provide some further discussion, also considering finite volume effects, in Section V.

$\mathbf{\Omega}:\ \mathbf{I(J^P) = 0(\frac{3}{2}^-)}$: In the $J^P = 3/2^-$ channel of the Ω baryons there is no experimental evidence. We find two states, both with a fairly good signal, in our simulations. The chiral extrapolation of the ground state energy level predicts a resonance slightly above 2 GeV (see Figure 13).

V. VOLUME DEPENDENCE OF BARYON ENERGY LEVELS

For resonance states in large volumes, there are two leading mechanisms of finite volume effects. For one, the spectral density of scattering states depends on the volume and distorts the energy spectrum through avoided level crossings. This mechanism is very important for the determination of resonance properties [2, 54]. The expected distortion from this effect is of $\mathcal{O}(\Gamma)$, where Γ is the width of the resonance. Notice that the resonance width is expected to be quite a bit smaller than the physical one at unphysical pion masses. This justifies identifying the pattern of energy levels qualitatively with the spectrum of resonances. Therefore, this kind of finite volume effect is discussed only qualitatively for particular observables. A second volume effect comes from virtual pion exchange with the mirror image. The so-called "pion wrapping around the universe" causes an exponential correction to the energy level of the hadron [55]. This mechanism can be discussed to higher orders in Chiral Perturbation Theory [56–58]. Here we follow a fit form successfully applied in [59],

$$E_h(L) = E_h(L=\infty) + c_h(m_\pi)\mathrm{e}^{-m_\pi L}(m_\pi L)^{-3/2}\ , \quad (3)$$

where E_h is the energy level of the hadron at linear size L of the lattice. It was suggested that $c_h(m_\pi) = c_{h,0}m_\pi^2$, which implies two fit parameters for each observable: $E_h(L = \infty)$ and $c_{h,0}$. The parameter $c_{h,0}$ is shared among different ensembles, which we exploit to make combined fits. We remark that the fit form used is a fairly simple one, however, considering the small number of different volumes, we have to rely on a method which uses few parameters.

Due to the exponential behavior, finite volume effects are expected to become non-negligible for $m_\pi L \lesssim 4$. This region is entered in particular for the ensembles with small pion masses. Eq. (3) is valid only for asymptotically large volumes, power-like corrections are expected for $m_\pi L \lesssim 3$ and already earlier for higher excitations. For ensemble C77 ($m_\pi = 330$ MeV) we generated data on configuration size $12^3 \times 24$, $16^3 \times 32$, and $24^3 \times 48$, for ensemble A66 ($m_\pi = 255$ MeV) we have data for size $16^3 \times 32$ and $24^3 \times 48$. All these ensembles, $2.7 < m_\pi L < 6$, where the pion cloud exchange should have a measurable effect described by Eq. (3). We apply Eq. (3) separately to each observable. The data of sets A66 and C77 enter a combined fit, and the resulting parameters are used to extrapolate the data of all ensembles (for that observable) to infinite volume. Finally, the results are extrapolated to the physical light-quark mass.

We focus on narrow or stable states with a good signal where clear finite volume effects can be expected. This is the case in particular for the ground states of the positive parity baryon channels. As mentioned in the previous section, the results for strange baryons are affected by our imperfect strange quark tuning. The tuning is of acceptable quality for 5 out of the 7 ensembles of size $16^3 \times 32$. We therefore omit the data from C64 and A66 for our final chiral fits for baryons with strangeness. As our tuning was done in finite volume the resulting value for the $\Omega(1672)$ will still deviate from the physical value. Assuming a simple dependence on the number of strange quarks, this deviation can be translated to other states and we provide this simple estimate as a second uncertainty when citing final values for the baryon masses. These values are also listed in Table VII.

A. Nucleon

$\mathbf{N}:\ \mathbf{I(J^P) = \frac{1}{2}(\frac{1}{2}^+)}$:

The nucleon spin $1/2^+$ ground state shows a very clean signal. Our result for the finite box of roughly 2.2 fm deviates significantly from experiment (see Fig. 2). In order to estimate the systematic error we compare two sets of interpolators A=(1,2,9,10,19,20) and B=(3,4,10,11,19,20). Furthermore, we consider different starting values for the fit range for the eigenvalues. The results for the different ensembles and the corresponding infinite volume extrapolations are shown in Fig. 14. Note that the result for (B,7) of ensemble A66 lies outside the

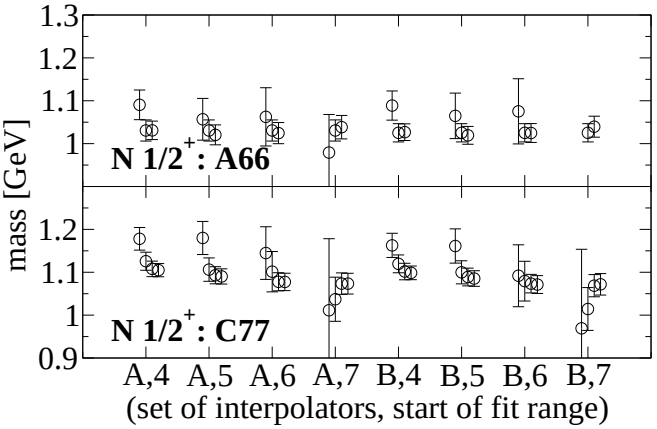

FIG. 14: Systematic error of the nucleon ground state energy level. The levels are shown for different choices of interpolators and fit ranges, labeled on the horizontal axis. E.g., "A4" denotes the set of interpolator "A" and a fit range for the eigenvalues from $t = 4a$ to the onset of noise. "A" denotes set of interpolators (1,2,9,10,19,20), "B" denotes (3,4,11,12,19,20). For each set of interpolator and fit range, results for small to large lattices (spatial size 16, 24 for ensemble A66, and 12,16, 24 for C77) are shown from left to right, the corresponding infinite volume limit rightmost.

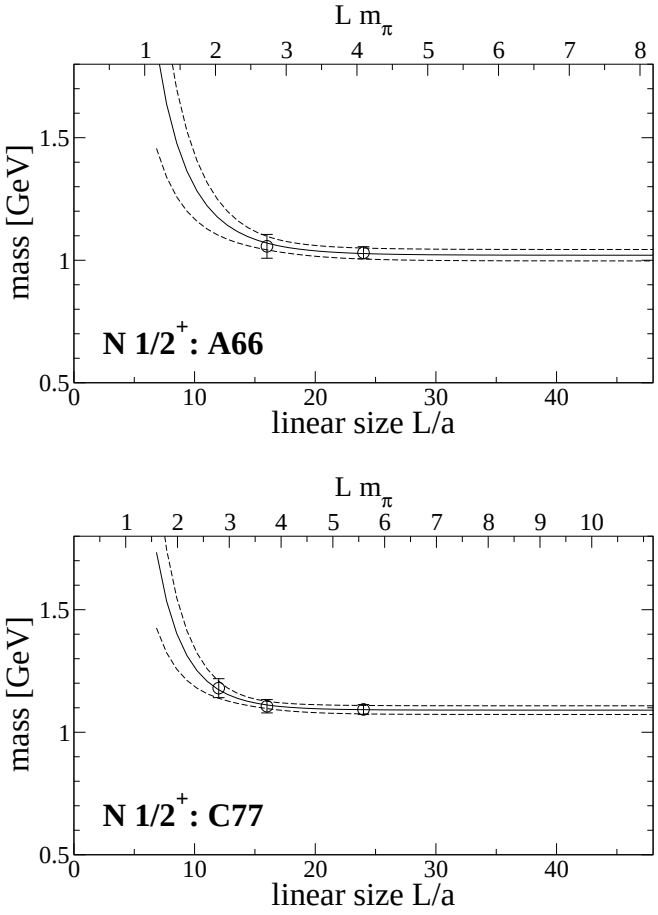

FIG. 15: Volume dependence of the nucleon mass for the set of interpolators (1,2,9,10,19,20) and $t_{\rm min} = 5a$ ((A,5) of Fig. 14).

plotted region. We conclude that for small volumes late starts of the fit have to be avoided.

We find a clear dependence of the nucleon energy level on the lattice volume. For definiteness, we choose the set of interpolators A and $t_{\rm min} = 5a$ and the corresponding infinite volume extrapolation, which is shown in Fig. 15. After infinite volume extrapolation of all ensembles with the extrapolation parameters determined from A66 and C77, we extrapolate to the physical pion mass, shown in Fig. 16 (upper). Our final result is $m_N = 954(16)$ MeV (error is statistical only), which agrees with the experimental $N(939)$ within 1σ.

$\mathbf{N}: \ \mathbf{I}(\mathbf{J^P}) = \frac{\mathbf{1}}{\mathbf{2}}(\frac{\mathbf{1}}{\mathbf{2}}^-)$:

In the nucleon spin $1/2^-$ channel we analyze the finite volume effects of the two lowest energy levels. Our results for the finite box of roughly 2.2 fm are a bit low compared to experiment (see Fig. 2). We show results for different volumes and infinite volume extrapolations for the ground state in Fig. 17 and for the first excitation in Fig. 18. Note that in some cases the data suggest negative finite volume corrections to the energy level. Such are compatible with an attractive s wave scattering state πN. However, the pattern is not systematically observed in A66 and C77, neither with nor without assuming a level crossing (with changing pion mass). Hence the finite volume analysis does not provide clear information on the particle content of the two lowest energy levels in the nucleon spin $1/2^-$ channel.

In fact, as has been shown recently in a study which includes meson-baryon interpolators [10], the spectrum should exhibit a sub-threshold energy level in addition to two levels close the the resonance position. Comparison of these results with the energy levels obtained here leads one to interpret the present eigenstates as superpositions of those states.

B. Delta Baryons

We show results and infinite volume extrapolations for different sets of interpolators and different fit ranges for the Δ spin $3/2^+$ ground state in Fig. 19. Compared to the nucleon, the fit ranges of the eigenvalues are short, correspondingly, and the results tend to fluctuate a bit more. The volume dependence appears to be the strongest of all observables considered. For definiteness, we choose the set of interpolators A and $t_{\rm min} = 5\,a$ and the corresponding infinite volume extrapolation, and note that the systematic error is of the order of the statistical error, or slightly larger. After infinite volume extrapolation of all ensembles, we extrapolate to the physical pion mass as shown in Fig. 16. Our final result is $m_\Delta = 1268(32)$ MeV, which agrees with the experimental $\Delta(1232)$ within roughly 1σ. We remark that the energy level in ensemble A66 appears low compared to other ensembles. This de-

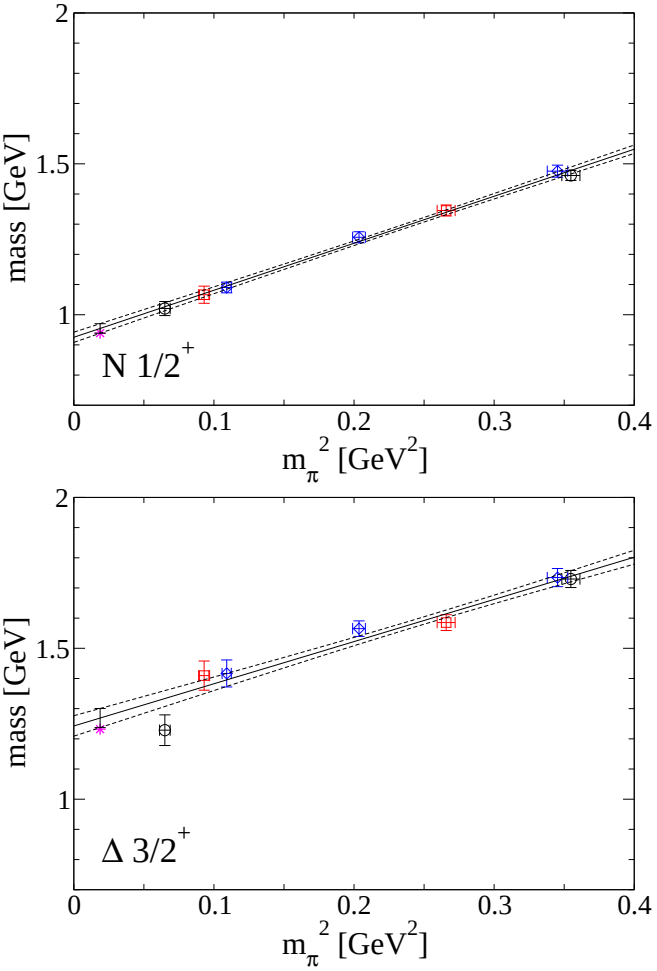

FIG. 16: Energy levels for the nucleon spin $\frac{1}{2}^+$ (upper) and Δ spin $\frac{3}{2}^+$ (lower) in the infinite volume limit. After infinite volume extrapolation ((A,5) of Fig. 14 resp. Fig. 19), we extrapolate to physical pion masses. We obtain m_N=954(16) MeV and m_Δ=1268(32) MeV, which both match the experimental values within roughly 1σ.

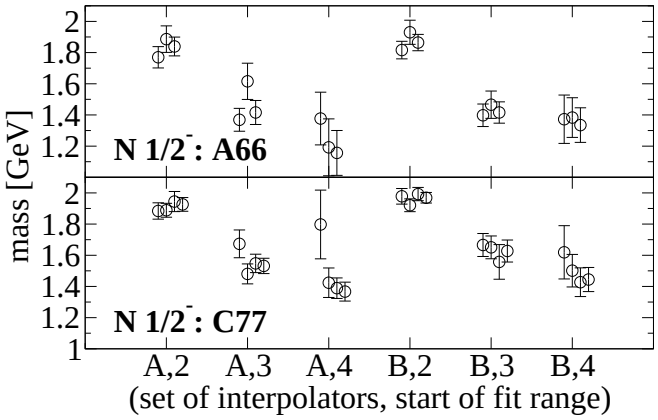

FIG. 17: Systematic error of the nucleon spin $1/2^-$ ground state mass, analogous to Fig. 14. "A" denotes set of interpolators (5,11,17), "B" denotes (1,2,9,10,17,18). For each set of interpolator and fit range, results for small to large lattices are shown from left to right, the corresponding infinite volume limit rightmost.

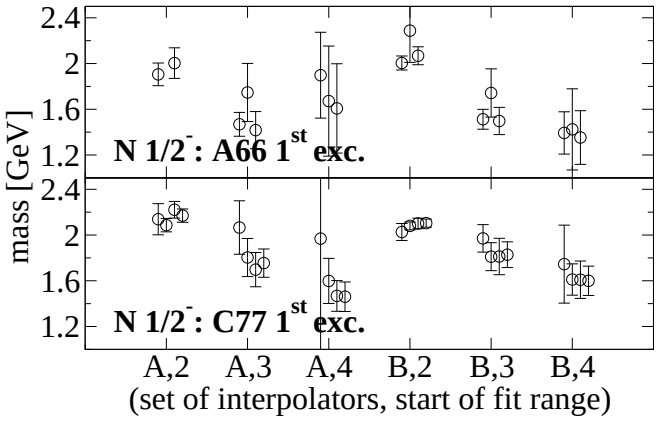

FIG. 18: Systematic error of the nucleon spin $1/2^-$ first excited energy level, analogous to Fig. 14. "A" denotes set of interpolators (5,11,17), "B" denotes (1,2,9,10,17,18). For each set of interpolator and fit range, results for small to large lattices are shown from left to right, the corresponding infinite volume limit rightmost.

grades the χ^2/d.o.f. of the chiral fit (see Table VII), but improves the comparison with experiment.

C. Omega Baryons

The Ω mass was used in the first place to define the strange quark mass parameter. We consider different sets of interpolators and fit ranges of the eigenvalues in order to estimate the corresponding systematic error. Figure 20 shows some of the corresponding results. Here, we choose for definiteness interpolators (1,3,4) and a fit range starting from $t_{\rm min} = 4a$ for the ensembles with letter C and $t_{\rm min} = 6a$ for the ensembles with letter A; we note that the corresponding systematic error appears to be somewhat smaller than the statistical one. We extrapolate the energy levels of all ensembles to infinite volume. In the final extrapolation to physical light-quark masses (see Fig. 21), we omit ensemble A66 and C64, because they show a slight mistuning in the strange quark mass. This strategy is also pursued for other strange baryons in the infinite volume limit. We obtain m_Ω = 1650(20) MeV, which agrees with the experimental $\Omega(1672)$ within 1.1 σ. The slight deviation originates from the quark mass tuning in finite volume using only partial statistics.

D. Sigma Baryons

In the Σ spin $1/2^+$ channel we apply the sets of interpolators A=(1,2,9,10,25,26) and B=(2,3,10,11,19,20,26,27) and different fit ranges to discuss the volume dependence of the ground state (see Fig. 23). The volume dependence

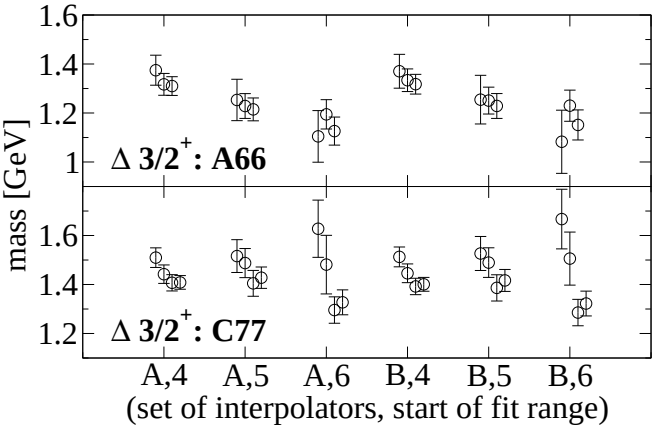

FIG. 19: Systematic error of the Δ spin $3/2^+$ mass, analogous to Fig. 14. "A" denotes set of interpolators (1,4,5), "B" denotes (1,5,8). For each set of interpolator and fit range, results for small to large lattices are shown from left to right, the corresponding infinite volume limit rightmost.

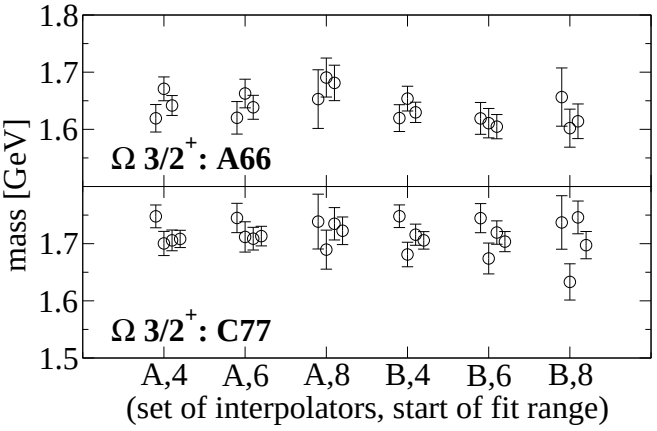

FIG. 20: Systematic error of the Ω spin $3/2^+$ mass, analogous to Fig. 14. "A" denotes set of interpolators (1,5,8), "B" denotes (1,3,4). For each set of interpolator and fit range, results for small to large lattices are shown from left to right, the corresponding infinite volume limit rightmost. For definiteness we choose (B,4).

is found to be comparable in size to the one of the nucleon ground state energy level. Towards larger fit ranges the results start to scatter; nevertheless, they are conclusive and the systematic error is of the order of the statistical one. We choose interpolators A and $t_{\rm min} = 6a$, and show the results in the infinite volume limit in the upper pane of Fig. 22. Our final result is $m_\Sigma = 1176(19)(+07)$ MeV (second error is a correction estimate based on the slight mistuning of the strange quark mass), which is compatible with the experimental Σ around 1193 MeV.

In the Σ spin $3/2^+$ channel we again use interpolators (2,3,10,11,12). The results are shown in the upper pane of Fig. 25. Here our final result is $m_\Sigma = 1431(25)(+07)$MeV which is somewhat larger than the experimental value of 1384 MeV.

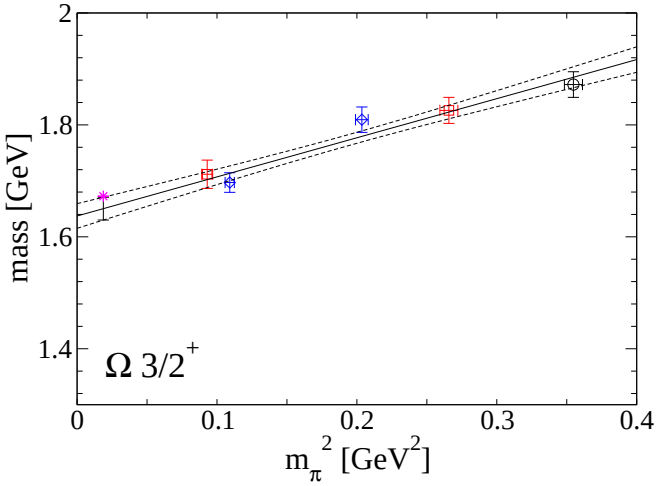

FIG. 21: Energy levels for Ω spin $3/2^+$ in the infinite volume limit. After infinite volume extrapolation we extrapolate to physical pion masses, obtaining m_Ω=1650(20) MeV. For discussion please refer to the text.

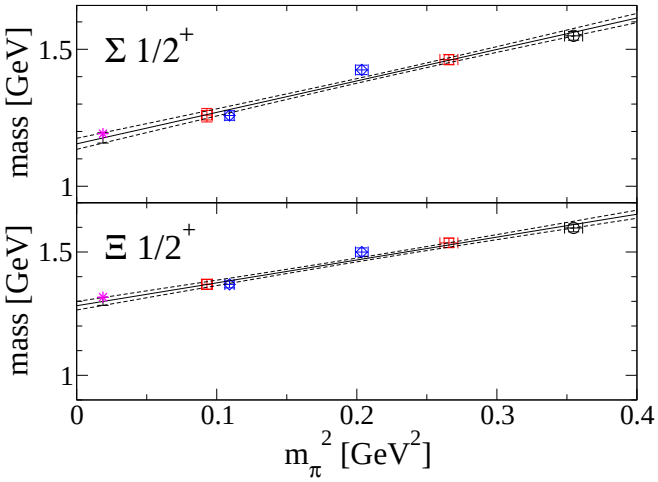

FIG. 22: Energy levels for the Σ spin $\frac{1}{2}^+$ (upper pane) and the Ξ spin $\frac{1}{2}^+$ (lower pane) ground states in the infinite volume limit. After infinite volume extrapolation we extrapolate to physical pion masses. We obtain m_Σ=1176(19)(+07) MeV and m_Ξ =1299(16)(+15) MeV.

E. Xi Baryons

We consider the sets of interpolators A=(1,2,9,10,25,26) and B=(2,3,10,11,19,20,26,27) and different fit ranges to discuss the volume dependence of the Ξ spin $1/2^+$ ground state (see Fig. 24). Again, the results are conclusive, and the systematic error is well bounded. We choose interpolators A and $t_{\rm min} = 6a$, and show the results for infinite volume in the upper pane of Fig. 25. Our final result is $m_\Xi = 1299(16)(+15)$ MeV which is again slightly lower than the experimental Ξ around 1317 MeV.

For the Ξ spin $3/2^+$ ground state we use interpo-

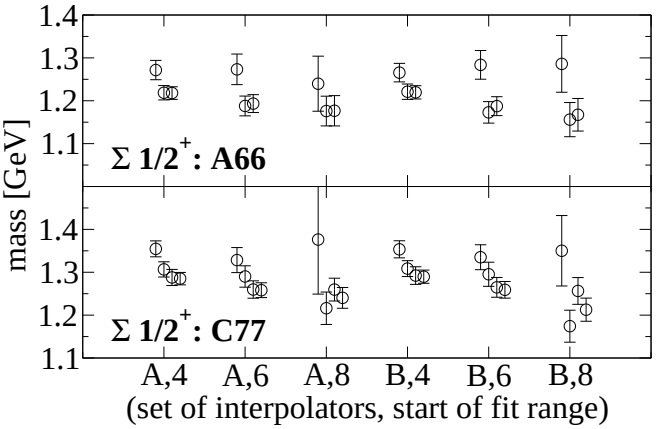

FIG. 23: Systematic error of the Σ spin $\frac{1}{2}^+$ mass, analogous to Fig. 14. "A" denotes set of interpolators (1,2,9,10,25,26), "B" denotes (2,3,10,11,19,20,26,27). For each set of interpolator and fit range, results for small to large lattices are shown from left to right, the corresponding infinite volume limit rightmost.

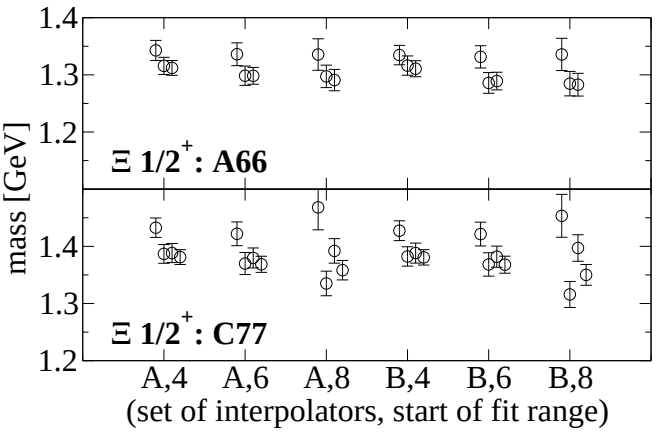

FIG. 24: Systematic error of the Ξ spin $1/2^+$mass, analogous to Fig. 14. "A" denotes set of interpolators (1,2,9,10,25,26), "B" denotes (2,3,10,11,19,20,26,27). For each set of interpolator and fit range, results for small to large lattices are shown from left to right, the corresponding infinite volume limit rightmost.

lators (2,3,10,11,12). The infinite volume results are shown in the right pane of Fig. 25. Our result is m_Ξ = 1540(22)(+15)MeV which is slightly larger than the experimental value 1532MeV.

VI. SUMMARY

We have derived results for the low lying energy levels in all baryon channels (spin 1/2 and 3/2, both parities) for baryons with light and strange valence quark content. The light quarks were included as dynamical quarks in the generation of gauge configurations by the hybrid Monte Carlo method. The quarks were implemented as

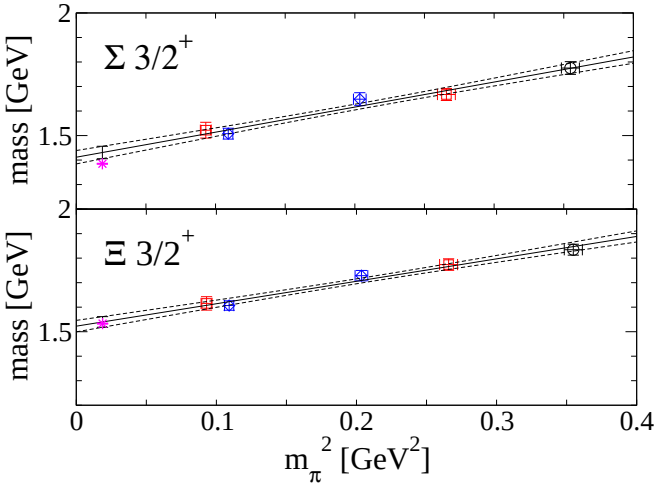

FIG. 25: Energy levels for Σ spin $3/2^+$ (upper pane) and Ξ spin $3/2^+$ (lower pane) ground states in the infinite volume limit. After infinite volume extrapolation we extrapolate to physical pion masses. We obtain m_Σ=1431(25)(+07) MeV and m_Ξ=1540(22)(+15) MeV.

Chirally Improved quarks, the pion masses range from 255 to 596 MeV.

Figure 26 shows our results for the extrapolation (leading order ChPT linear in m_π^2) of the finite volume energy levels to physical pion mass. We find good agreement of the ground state energy levels with the experimental values, where available. In some cases (e.g., in the Omega and the Ξ sectors) our results suggest the existence of yet unobserved resonance states. We use 3-quark interpolators for the baryons throughout and find no signal for a coupling to dynamically generated meson-baryon states in p- and d-wave channels. This is not so clear for the s wave channels. These show several energy levels close to ground states in the $\frac{1}{2}^-$ channels. In these cases there could be mixing with the s wave meson-baryon sectors.

We want to mention that for all our ensembles (i.e., over the whole pion mass range) the Gell-Mann–Okubo formula [60, 61] is fulfilled with high precision. The values of the combination of the spin 1/2 positive parity octet ground state masses obey

$$\left|\frac{2M_N + 2M_\Xi - M_\Sigma - 3M_\Lambda}{2M_N + 2M_\Xi + M_\Sigma + 3M_\Lambda}\right| < 0.03 \qquad (4)$$

for all pion masses studies here.

We analyze the flavor symmetry content by identifying the singlet/octet/decuplet contributions. For the ground states agreement with the expectations from the quark model is found. In the $\frac{1}{2}^+$ nucleon channel the first excitation is considerably higher than the Roper resonance and one possible interpretation is, that the physical state couples very weakly to our interpolators. This may be also the case in the $\Lambda\frac{1}{2}^+$ channel, where the first excitation is dominated by singlet interpolators matching the $\Lambda(1810)$ (singlet in the quark model) and the Roper-like

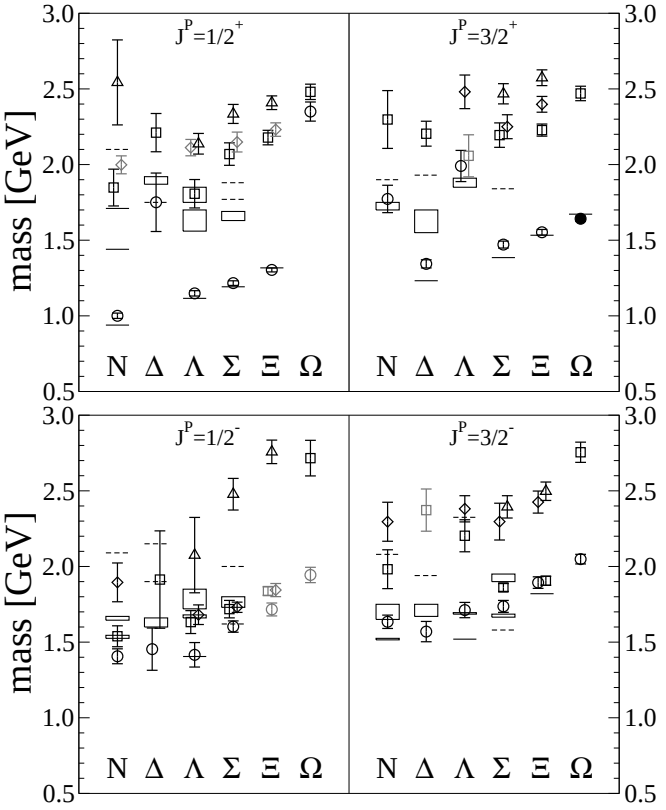

FIG. 26: Energy levels for positive parity (top) and negative parity baryons (bottom). All values are obtained by chiral extrapolation linear in the pion mass squared. Horizontal lines or boxes represent experimentally known states, dashed lines indicate poor evidence, according to [48]. The statistical uncertainty of our results is indicated by bands of 1σ, that of the experimental values by boxes of 1σ. The strange quarks are implemented in valence approximation. Grey symbols denote a poor χ^2/d.o.f. of the chiral fits (see Tables V and VI).

$\Lambda(1600)$ (octet in the quark model) seems to be missing.

We study the systematic errors due to the final choice of interpolator sets and fit ranges and we also perform infinite volume extrapolations for the lowest energy levels. Because a slight mistuning of the strange quark mass is identified in two of the ensembles, we omit them in the final extrapolation to the physical pion mass. Remaining small deviations are expected to stem from systematic effects which cannot be identified uniquely given our limited dataset at a single lattice spacing with 2 dynamical quark flavors. In general, however, our results in the infinite volume limit compare favorably with experiment, as shown in Fig. 27.

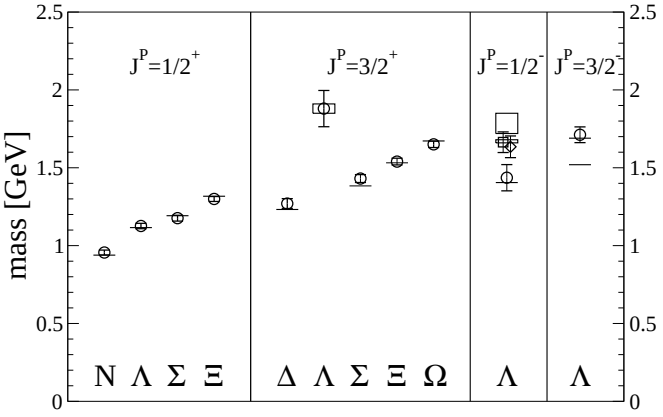

FIG. 27: Energy levels of baryons in the infinite volume limit at physical pion mass. Horizontal lines and boxes represent experimentally known states [48]. The statistical uncertainty of our results is indicated by bands of 1σ.

Acknowledgments

We would like to thank Elvira Gamiz, Christof Gattringer, Leonid Y. Glozman, Markus Limmer, Willibald Plessas, Helios Sanchis-Alepuz, Mario Schröck and Valentina Verduci for valuable discussions. The calculations have been performed on the SGI Altix 4700 of the Leibniz-Rechenzentrum Munich and on local clusters at UNI-IT at the University of Graz. We thank these institutions for providing support. G.P.E. was partially supported by the MIUR–PRIN contract 20093BMNPR. D.M. acknowledges support by Natural Sciences and Engineering Research Council of Canada (NSERC) and G.P.E. and A.S. acknowledge support by the DFG project SFB/TR-55. Fermilab is operated by Fermi Research Alliance, LLC under Contract No. De-AC02-07CH11359 with the United States Department of Energy.

Appendix A: Tables of Baryon Interpolators

All interpolators are projected to definite parity using the projector

$$P^{\pm} = \frac{1}{2}(\mathbb{1} \pm \gamma_t) \,. \tag{A1}$$

The resulting correlation matrices of positive and negative parity ($\pm$),

$$C_{ij}^{\pm}(t) = \pm Z_{ij}^{\pm} \mathrm{e}^{-tE^{\pm}} \pm Z_{ij}^{\mp} \mathrm{e}^{-(T-t)E^{\mp}}, \tag{A2}$$

are combined to the correlation matrices

$$C(t) = \frac{1}{2}\left(C^{+}(t) - C^{-}(T-t)\right) \,, \tag{A3}$$

which are then used in the variational method.

All Rarita-Schwinger fields (spin 3/2 interpolators of Table II) are projected to definite spin 3/2 using the continuum formulation of the Rarita-Schwinger projector [62]

$$P_{\mu\nu}^{3/2}(\vec{p}) = \delta_{\mu\nu} - \frac{1}{3}\gamma_\mu\gamma_\nu - \frac{1}{3p^2}(\gamma\cdot p\,\gamma_\mu p_\nu + p_\mu\gamma_\nu\gamma\cdot p) \,. \tag{A4}$$

The baryon interpolators used in this work are detailed in Tables II, III and IV. Table II shows the flavor structure for all interpolators. For the spin 1/2 channels of the nucleon, Σ, Ξ and Λ, we use the three different Dirac structures $\chi^{(i)} = (\Gamma_1^{(i)}, \Gamma_2^{(i)}), (i = 1, 2, 3)$, listed in Table III. Details about the quark smearings in the interpolators are found in Table IV. The name convention of all baryon interpolators is determined by Tables III and IV. In the Λ channels, singlet and octet interpolators are collected in one set. We assign to the first octet interpolator the number after the last singlet interpolator, and continue to count for the remaining octet interpolators. In the Σ and Ξ channels, the same holds for octet and decuplet interpolators.

In the continuum, the actual number of independent fields is reduced by Fierz identities. In particular, there are no non-vanishing point-like interpolators for $\Delta(\frac{1}{2})$ and singlet $\Lambda(\frac{3}{2})$. However, using differently smeared quarks in the construction of interpolators, we do access independent information and find good signals for the singlet $\Lambda(\frac{3}{2})$ propagation.

Appendix B: Tables of Energy Levels and χ^2

We give the results of our extrapolation (linear in m_π^2) to the physical pion mass together with the associated value of χ^2/d.o.f.

Spin	Flavor channel	Name	Interpolator
$\frac{1}{2}$	Nucleon	$N^{(i)}_{1/2}$	$\epsilon_{abc}\,\Gamma_1^{(i)}\,u_a\left(u_b^T\,\Gamma_2^{(i)}\,d_c - d_b^T\,\Gamma_2^{(i)}\,u_c\right)$
$\frac{1}{2}$	Delta	$\Delta_{1/2}$	$\epsilon_{abc}\,\gamma_i\gamma_5 u_a\left(u_b^T\,C\,\gamma_i\,u_c\right)$
$\frac{1}{2}$	Sigma octet	$\Sigma^{(8,i)}_{1/2}$	$\epsilon_{abc}\,\Gamma_1^{(i)}\,u_a\left(u_b^T\,\Gamma_2^{(i)}\,s_c - s_b^T\,\Gamma_2^{(i)}\,u_c\right)$
$\frac{1}{2}$	Sigma decuplet	$\Sigma^{(10,i)}_{1/2}$	$\epsilon_{abc}\,\gamma_i\gamma_5 u_a\left(u_b^T\,C\,\gamma_i\,s_c - s_b^T\,C\,\gamma_i\,u_c\right)$
$\frac{1}{2}$	Xi octet	$\Xi^{(8,i)}_{1/2}$	$\epsilon_{abc}\,\Gamma_1^{(i)}\,s_a\left(s_b^T\,\Gamma_2^{(i)}\,u_c - u_b^T\,\Gamma_2^{(i)}\,s_c\right)$
$\frac{1}{2}$	Xi decuplet	$\Xi^{(10,i)}_{1/2}$	$\epsilon_{abc}\,\gamma_i\gamma_5 s_a\left(s_b^T\,C\,\gamma_i\,u_c - u_b^T\,C\,\Gamma_i\,s_c\right)$
$\frac{1}{2}$	Lambda singlet	$\Lambda^{(1,i)}_{1/2}$	$\epsilon_{abc}\Gamma_1^{(i)}u_a(d_b^T\Gamma_2^{(i)}s_c - s_b^T\Gamma_2^{(i)}d_c)$ $+\,\text{cyclic permutations of } u,d,s$
$\frac{1}{2}$	Lambda octet	$\Lambda^{(8,i)}_{1/2}$	$\epsilon_{abc}\Big[\Gamma_1^{(i)}s_a(u_b^T\Gamma_2^{(i)}d_c - d_b^T\Gamma_2^{(i)}u_c)$ $+\,\Gamma_1^{(i)}u_a(s_b^T\Gamma_2^{(i)}d_c) - \Gamma_1^{(i)}d_a(s_b^T\Gamma_2^{(i)}u_c)\Big]$
$\frac{1}{2}$	Omega	$\Omega_{1/2}$	$\epsilon_{abc}\,\gamma_i\gamma_5 s_a\left(s_b^T\,C\,\gamma_i\,s_c\right)$
$\frac{3}{2}$	Nucleon	$N^{(i)}_{3/2}$	$\epsilon_{abc}\,\gamma_5\,u_a\left(u_b^T\,C\gamma_5\gamma_i\,d_c - d_b^T\,C\gamma_5\gamma_i\,u_c\right)$
$\frac{3}{2}$	Delta	$\Delta^{(i)}_{3/2}$	$\epsilon_{abc}\,u_a\left(u_b^T\,C\,\gamma_i\,u_c\right)$
$\frac{3}{2}$	Sigma octet	$\Sigma^{(8,i)}_{3/2}$	$\epsilon_{abc}\,\gamma_5\,u_a\left(u_b^T\,C\gamma_5\gamma_i\,s_c - s_b^T\,C\gamma_5\gamma_i\,u_c\right)$
$\frac{3}{2}$	Sigma decuplet	$\Sigma^{(10,i)}_{3/2}$	$\epsilon_{abc}\,u_a\left(u_b^T\,C\gamma_i\,s_c - s_b^T\,C\gamma_i\,u_c\right)$
$\frac{3}{2}$	Xi octet	$\Xi^{(8,i)}_{3/2}$	$\epsilon_{abc}\,\gamma_5\,s_a\left(s_b^T\,C\gamma_5\gamma_i\,u_c - u_b^T\,C\gamma_5\gamma_i\,s_c\right)$
$\frac{3}{2}$	Xi decuplet	$\Xi^{(10,i)}_{3/2}$	$\epsilon_{abc}\,s_a\left(s_b^T\,C\gamma_i\,u_c - u_b^T\,C\gamma_i\,s_c\right)$
$\frac{3}{2}$	Lambda singlet	$\Lambda^{(1,i)}_{3/2}$	$\epsilon_{abc}\gamma_5 u_a(d_b^T C\gamma_5\gamma_i s_c - s_b^T C\gamma_5\gamma_i d_c)$ $+\,\text{cyclic permutations of } u,d,s$
$\frac{3}{2}$	Lambda octet	$\Lambda^{(8,i)}_{3/2}$	$\epsilon_{abc}\Big[\gamma_5 s_a(u_b^T C\gamma_5\gamma_i d_c - d_b^T C\gamma_5\gamma_i u_c)$ $+\,\gamma_5 u_a(s_b^T C\gamma_5\gamma_i d_c) - \gamma_5 d_a(s_b^T C\gamma_5\gamma_i u_c\Big]$
$\frac{3}{2}$	Omega	$\Omega^{(i)}_{3/2}$	$\epsilon_{abc}\,s_a\left(s_b^T\,C\,\gamma_i\,s_c\right)$

TABLE II: Baryon interpolators: Flavor structure. The possible choices for the Dirac matrices $\Gamma^{(i)}_{1,2}$ in the spin 1/2 channels are listed in Table III. All interpolators are projected to definite parity according to Eq. (A1). All spin 3/2 interpolators include the Rarita-Schwinger projector, according to Eq. (A4), which is suppressed for clarity in the table. C denotes the charge conjugation matrix, γ_i the spatial Dirac matrices and γ_t the Dirac matrix in time direction. Spin 1/2 and spin 3/2 channels are separated by a solid line. Summation convention applies for repeated indices, and in the case of spin 3/2 observables, the open Lorentz index (after spin projection) is summed after taking the expectation value of correlation functions.

i	$\Gamma_1^{(i)}$	$\Gamma_2^{(i)}$	Numbering of associated interpolators $N_{1/2}, \Lambda^1_{1/2}, \Sigma^8_{1/2}, \Xi^8_{1/2}$	$\Lambda^8_{1/2}, \Sigma^{10}_{1/2}, \Xi^{10}_{1/2}$
1	$\mathbb{1}$	$C\gamma_5$	1-8	25-32
2	γ_5	C	9-16	33-40
3	$i\mathbb{1}$	$C\gamma_t\gamma_5$	17-24	41-48

TABLE III: Baryon interpolators: Dirac structures used for the spin 1/2 nucleon, Λ, Σ and Ξ interpolators, according to Table II. The naming convention (numbering) for associated interpolators in the different channels is given as well. The subscripts denote the spin, the superscripts the flavor irreducible representation.

quark smearing	Numbering of associated interpolators $\Delta_{1/2}, \Delta_{3/2}$ $\Omega_{1/2}, \Omega_{3/2}$, $N_{3/2}, \Lambda^1_{3/2}$ $\Sigma^8_{3/2}, \Xi^8_{3/2}$	$\Lambda^8_{3/2}$, $\Sigma^{10}_{3/2}$, $\Xi^{10}_{3/2}$	$N_{1/2}, \Lambda^1_{1/2}$, $\Sigma^8_{1/2}, \Xi^8_{1/2}$	$\Lambda^8_{1/2}$, $\Sigma^{10}_{1/2}, \Xi^{10}_{1/2}$
(nn)n	1	9	1,9,17	25,33,41
(nn)w	2	10	2,10,18	26,34,42
(nw)n	3	11	3,11,19	27,35,43
(nw)w	4	12	4,12,20	28,36,44
(wn)n	5	13	5,13,21	29,37,45
(wn)w	6	14	6,14,22	30,38,46
(ww)n	7	15	7,15,23	31,39,47
(ww)w	8	16	8,16,24	32,40,48

TABLE IV: Baryon interpolators: Quark smearing types and naming convention for the interpolators in the different channels. The subscripts denotes the spin, the superscripts the flavor irreducible representation. The brackets in the first row symbolize the diquark part. Due to Fierz identities, some of the interpolators may be linearly dependent.

Baryon: $I(J^P)$	Energy level [MeV]	χ^2/d.o.f.
$N: 1/2(1/2^+)$	1000(18)	2.16/5
$N: 1/2(1/2^+)$	1848(120)	3.61/5
$N: 1/2(1/2^+)$	1998(59)	18.31/5
$N: 1/2(1/2^+)$	2543(280)	1.96/3
$\Delta: 3/2(1/2^+)$	1751(190)	1.58/5
$\Delta: 3/2(1/2^+)$	2211(126)	1.15/5
$\Lambda: 0(1/2^+)$	1149(18)	1.89/3
$\Lambda: 0(1/2^+)$	1807(94)	4.63/5
$\Lambda: 0(1/2^+)$	2112(54)	20.27/5
$\Lambda: 0(1/2^+)$	2137(68)	1.50/5
$\Sigma: 1(1/2^+)$	1216(15)	6.94/5
$\Sigma: 1(1/2^+)$	2069(74)	3.41/5
$\Sigma: 1(1/2^+)$	2149(66)	20.37/5
$\Sigma: 1(1/2^+)$	2335(63)	2.09/5
$\Xi: 1/2(1/2^+)$	1303(13)	8.31/5
$\Xi: 1/2(1/2^+)$	2178(48)	7.51/5
$\Xi: 1/2(1/2^+)$	2231(44)	26.53/5
$\Xi: 1/2(1/2^+)$	2408(45)	10.37/5
$\Omega: 0(1/2^+)$	2350(63)	4.14/5
$\Omega: 0(1/2^+)$	2481(51)	4.35/5
$N: 1/2(3/2^+)$	1773(91)	8.35/5
$N: 1/2(3/2^+)$	2298(191)	3.79/5
$\Delta: 3/2(3/2^+)$	1344(27)	6.13/5
$\Delta: 3/2(3/2^+)$	2204(82)	6.23/5
$\Lambda: 0(3/2^+)$	1991(103)	3.56/3
$\Lambda: 0(3/2^+)$	2058(139)	23.04/5
$\Lambda: 0(3/2^+)$	2481(111)	4.26/5
$\Sigma: 1(3/2^+)$	1471(23)	2.52/5
$\Sigma: 1(3/2^+)$	2194(81)	4.78/5
$\Sigma: 1(3/2^+)$	2250(79)	7.05/5
$\Sigma: 1(3/2^+)$	2468(67)	4.22/5
$\Xi: 1/2(3/2^+)$	1553(18)	3.78/5
$\Xi: 1/2(3/2^+)$	2228(40)	6.99/5
$\Xi: 1/2(3/2^+)$	2398(52)	7.03/5
$\Xi: 1/2(3/2^+)$	2574(52)	4.26/5
$\Omega: 0(3/2^+)$	1642(17)	10.86/5
$\Omega: 0(3/2^+)$	2470(49)	8.14/5

TABLE V: Energy levels at the physical pion mass and corresponding χ^2/d.o.f. for the chiral fits of the positive baryon energy levels reported in this work. Sources of large χ^2/d.o.f. (≥ 3) are discussed in the text. Spin 1/2 and spin 3/2 baryons are separated by a line. Given errors are statistical only.

Baryon: $I(J^P)$	Energy level [MeV]	χ^2/d.o.f.
$N: 1/2(1/2^-)$	1406(49)	6.51/5
$N: 1/2(1/2^-)$	1539(69)	8.72/5
$N: 1/2(1/2^-)$	1895(128)	6.35/5
$N: 1/2(1/2^-)$	1918(211)	5.94/5
$\Delta: 3/2(1/2^-)$	1454(140)	11.16/5
$\Delta: 3/2(1/2^-)$	1914(322)	3.24/5
$\Lambda: 0(1/2^-)$	1416(81)	1.25/3
$\Lambda: 0(1/2^-)$	1546(110)	0.57/3
$\Lambda: 0(1/2^-)$	1713(116)	3.49/3
$\Lambda: 0(1/2^-)$	2075(249)	13.56/5
$\Sigma: 1(1/2^-)$	1603(38)	7.45/5
$\Sigma: 1(1/2^-)$	1718(58)	12.78/5
$\Sigma: 1(1/2^-)$	1730(34)	10.79/5
$\Sigma: 1(1/2^-)$	2478(104)	11.94/5
$\Xi: 1/2(1/2^-)$	1716(43)	19.10/5
$\Xi: 1/2(1/2^-)$	1837(28)	20.25/5
$\Xi: 1/2(1/2^-)$	1844(43)	15.75/5
$\Xi: 1/2(1/2^-)$	2758(78)	5.61/5
$\Omega: 0(1/2^-)$	1944(56)	20.48/5
$\Omega: 0(1/2^-)$	2716(118)	8.58/5
$N: 1/2(3/2^-)$	1634(44)	14.75/5
$N: 1/2(3/2^-)$	1982(128)	7.40/5
$N: 1/2(3/2^-)$	2296(129)	9.59/5
$\Delta: 3/2(3/2^-)$	1570(67)	4.01/5
$\Delta: 3/2(3/2^-)$	2373(140)	17.97/5
$\Lambda: 0(3/2^-)$	1751(41)	1.42/3
$\Lambda: 0(3/2^-)$	2203(106)	3.97/5
$\Lambda: 0(3/2^-)$	2381(87)	6.48/5
$\Sigma: 1(3/2^-)$	1861(26)	6.33/5
$\Sigma: 1(3/2^-)$	1736(40)	2.25/5
$\Sigma: 1(3/2^-)$	2394(74)	9.73/5
$\Sigma: 1(3/2^-)$	2297(122)	3.90/5
$\Xi: 1/2(3/2^-)$	1906(29)	3.12/5
$\Xi: 1/2(3/2^-)$	1894(38)	3.19/5
$\Xi: 1/2(3/2^-)$	2497(61)	8.53/5
$\Xi: 1/2(3/2^-)$	2426(73)	7.60/5
$\Omega: 0(3/2^-)$	2049(32)	7.32/5
$\Omega: 0(3/2^-)$	2755(67)	5.68/5

TABLE VI: Same as Table V, but for negative parity baryons. Spin 1/2 and spin 3/2 baryons are separated by a line.

Hadron	$I(J^P)$	Energy level [MeV]	χ^2/d.o.f.
N	$1/2(1/2^+)$	954(16)	2.26/5
Λ	$0(1/2^+)$	1126(17)(+07)	2.74/3
Σ	$1(1/2^+)$	1176(19)(+07)	6.67/3
Ξ	$1/2(1/2^+)$	1299(16)(+15)	5.05/3
Δ	$3/2(3/2^+)$	1268(32)	8.67/5
Λ	$0(3/2^+)$	1880(116)(+07)	2.38/3
Σ	$1(3/2^+)$	1431(25)(+07)	2.29/3
Ξ	$1/2(3/2^+)$	1540(22)(+15)	2.05/3
Ω	$0(3/2^+)$	1650(20)(+22)	3.10/3
Λ	$0(1/2^-)$	1436(84)(+07)	1.25/3
Λ	$0(1/2^-)$	1635(70)(+07)	4.93/3
Λ	$0(1/2^-)$	1664(66)(+07)	3.49/3
Λ	$0(3/2^-)$	1712(51)(+07)	2.92/3

TABLE VII: Same as Table V, but for hadrons after the infinite volume extrapolation. The horizontal line separates different parity and spin. Notice that the Omega mass is not a prediction of our calculation. The second errors given are naïve estimates for the systematic error from a mistuning of the strange quark mass.

[1] M. Lüscher, Nucl. Phys. B **354**, 531 (1991).
[2] M. Lüscher, Nucl. Phys. B **364**, 237 (1991).
[3] J. Bulava, *et al.*, Phys. Rev. D **82**, 014507 (2010), arXiv:1004.5072 [hep-lat].
[4] G. P. Engel, C. B. Lang, M. Limmer, D. Mohler, and A. Schäfer, Phys. Rev. D **82**, 034505 (2010), arXiv:1005.1748 [hep-lat].
[5] G. P. Engel, C. B. Lang, and A. Schäfer, Phys. Rev. D **87**, 034503 (2013), arXiv:1212.2032 [hep-lat] .
[6] C. B. Lang, D. Mohler, S. Prelovsek, and M. Vidmar, Phys. Rev. D **84**, 054503 (2011), arXiv:1105.5636 [hep-lat] .
[7] C. B. Lang, L. Leskovec, D. Mohler, and S. Prelovsek, Phys. Rev. D **86**, 054508 (2012), arXiv:1207.3204 [hep-lat].
[8] M. Göckeler, et al., Phys. Rev. D **86**, 094513 (2012), arXiv:1206.4141 [hep-lat].
[9] J. M. M. Hall, A. C. P. Hsu, D. B. Leinweber, A. W. Thomas, and R. D. Young, PoS **LATTICE2012**, 145 (2012), 1207.3562 .
[10] C. B. Lang and V. Verduci, Phys. Rev. D **87**, 054502 (2013), 1212.5055 .
[11] C. Gattringer, Phys. Rev. D **63**, 114501 (2001), arXiv:hep-lat/0003005.
[12] C. Gattringer, I. Hip, and C. B. Lang, Nucl. Phys. B **597**, 451 (2001), arXiv:hep-lat/0007042.
[13] A. Walker-Loud, *et al.*, Phys. Rev. D **79**, 054502 (2009), arXiv:0806.4549 [hep-lat] .
[14] A. Walker-Loud, PoS **LATTICE 2008**, 005 (2008), arXiv:0810.0663 [hep-lat].
[15] J. Bulava, et al., Phys. Rev. D **79**, 034505 (2009), arXiv:0901.0027 [hep-lat].
[16] J. Bulava, *et al.*, PoS **LATTICE2011**, 131 (2011), arXiv:1111.0845 [hep-lat].
[17] R. G. Edwards, J. J. Dudek, D. G. Richards, and S. J. Wallace, Phys. Rev. D **84**, 074508 (2011), arXiv:1104.5152 [hep-ph].
[18] M. S. Mahbub, W. Kamleh, D. B. Leinweber, P. J. Moran, and A. G. Williams, Phys.Lett. **B707**, 389 (2012), arXiv:1011.5724 [hep-lat].
[19] M. S. Mahbub, W. Kamleh, D. B. Leinweber, P. J. Moran, and A. G. Williams, PoS **LATTICE2010**, 112 (2010), arXiv:1011.0480 [hep-lat].
[20] B. J. Menadue, W. Kamleh, D. B. Leinweber, and M. S. Mahbub, Phys. Rev. Lett. **108**, 112001 (2012), arXiv:1109.6716 [hep-lat].
[21] M. S. Mahbub, W. Kamleh, D. B. Leinweber, P. J. Moran, and A. G. Williams, "Low-lying Odd-parity States of the Nucleon in Lattice QCD," (2012), arXiv:1209.0240 [hep-lat].
[22] C. Alexandrou, *et al.*, Phys. Rev. D **86**, 114501 (2012), arXiv:1205.6856 [hep-lat].
[23] R. Arthur, *et al.*, "Domain Wall QCD with Near-Physical Pions," (2012), arXiv:1208.4412 [hep-lat].
[24] R. G. Edwards, N. Mathur, D. G. Richards, and S. J. Wallace, "The Flavor Structure of the Excited Baryon Spectra from Lattice QCD," (2012), arXiv:1212.5236 [hep-lat] .
[25] J. Bulava, PoS **LATTICE2011**, 021 (2011), arXiv:1112.0212 [hep-lat].
[26] H. W. Lin, Chin. J. Phys. **49**, 827 (2011), arXiv:1106.1608 [hep-lat].
[27] Z. Fodor and C. Hoelbling, Rev.Mod.Phys. **84**, 449 (2012), arXiv:1203.4789 [hep-lat].
[28] C. Gattringer, *et al.*, Nucl. Phys. B **677**, 3 (2004), arXiv:hep-lat/0307013.
[29] T. Burch, *et al.*, Phys. Rev. D **74**, 014504 (2006), arXiv:hep-lat/0604019.
[30] C. B. Lang, P. Majumdar, and W. Ortner, Phys. Rev. D **73**, 034507 (2006), arXiv:hep-lat/0512014.
[31] C. Gattringer, C. Hagen, C. B. Lang, M. Limmer, D. Mohler, and A. Schäfer, Phys. Rev. D **79**, 054501 (2009), arXiv:0812.1681 [hep-lat] .
[32] C. Morningstar and M. Peardon, Phys. Rev. D **69**, 054501 (2004), arXiv:hep-lat/0311018.
[33] M. Lüscher and P. Weisz, Commun. Math. Phys. **97**, 59 (1985).
[34] G. P. Engel, C. B. Lang, M. Limmer, D. Mohler, and A. Schäfer, Phys. Rev. D **85**, 034508 (2012), arXiv:1112.1601 [hep-lat] .
[35] P. Fritzsch, *et al.*, Nucl. Phys. B **865**, 397 (2012), arXiv:1205.5380 [hep-lat].
[36] G. Bali, *et al.*, Nucl. Phys. B **866**, 1 (2013), arXiv:1206.7034 [hep-lat].
[37] S. Duane, A. D. Kennedy, B. J. Pendleton, and D. Roweth, Phys. Lett. B **195**, 216 (1987).
[38] M. Lüscher and U. Wolff, Nucl. Phys. B **339**, 222 (1990).
[39] C. Michael, Nucl. Phys. B **259**, 58 (1985).
[40] B. Blossier, M. DellaMorte, G. von Hippel, T. Mendes, and R. Sommer, JHEP **0904**, 094 (2009), arXiv:0902.1265 [hep-lat].
[41] N. Isgur and G. Karl, Phys. Rev. D **18**, 4187 (1978).
[42] N. Isgur and G. Karl, Phys. Rev. D **19**, 2653 (1979).
[43] L. Y. Glozman and D. O. Riska, Phys. Rept. **268**, 263 (1996), arXiv:hep-ph/9505422.
[44] S. Capstick and N. Isgur, Phys. Rev. **34**, 2809 (1986).
[45] L. Y. Glozman, W. Plessas, K. Varga, and R. Wagenbrunn, Phys. Rev. D **58**, 094030 (1998), arXiv:hep-ph/9706507 [hep-ph].
[46] U. Löring, B. C. Metsch, and H. R. Petry, Eur.Phys.J. **A10**, 395 (2001), arXiv:hep-ph/0103289 [hep-ph] .
[47] T. Melde, W. Plessas, and B. Sengl, Phys. Rev. D **77**, 114002 (2008), arXiv:0806.1454 [hep-ph].
[48] J. Beringer, *et al.* (Particle Data Group), Phys. Rev. D **86**, 010001 (2012).
[49] N. Isgur and G. Karl, Phys.Lett. **B72**, 109 (1977).
[50] S. Cohen, *et al.* , PoS **LAT2009**, 112 (2009), arXiv:0911.3373 [hep-lat].
[51] M. S. Mahbub, *et al.* PoS **LAT2009**, 118 (2009), arXiv:0910.2789 [hep-lat].
[52] T. T. Takahashi and M. Oka, PoS **LAT2009**, 108 (2009), arXiv:0911.2542 [hep-lat].
[53] T. T. Takahashi and M. Oka, Phys. Rev. D **81**, 034505 (2010), arXiv:0910.0686 [hep-lat].
[54] M. Lüscher, Commun. Math. Phys. **105**, 153 (1986).
[55] M. Lüscher, Commun. Math. Phys. **104**, 177 (1986).
[56] G. Colangelo, S. Dürr, and C. Haefeli, Nucl. Phys. B **721**, 136 (2005), hep-lat/0503014 .

[57] G. Colangelo, A. Fuhrer, and C. Haefeli, Nucl. Phys. Proc. Suppl. **153**, 41 (2006), arXiv:hep-lat/0512002.
[58] U.-G. Meissner, PoS **LAT2005**, 009 (2006), hep-lat/0509029.
[59] S. Dürr, *et al.*, Science **322**, 1224 (2008), arXiv:0906.3599 [hep-lat].
[60] M. Gell-Mann, CTSL-20, TID-12608 "The Eightfold Way: A Theory of Strong Interaction Symmetry," (1961).
[61] S. Okubo, Prog.Theor.Phys. **27**, 949 (1962).
[62] D. Lurié, *Particles and Fields* (Interscience Publishers, 1968).